Review article

Mineralogy, geochemistry and occurrences of fougerite in a modern hydrothermal system and its implications for the origin of life

Fabienne Trolard [a,b,c,*], Simon Duval [d], Wolfgang Nitschke [d], Bénédicte Ménez [e], Céline Pisapia [e], Jihaine Ben Nacib [a,g], Muriel Andréani [f], Guilhem Bourrié [a,b,c]

[a] INRAE, UMR 1114 Emmah, 84914, Avignon cedex 9, France
[b] Avignon University, UMR 1114 Emmah, 84914, Avignon cedex 9, France
[c] Académie d'Agriculture de France, Paris, 75007, France
[d] Aix-Marseille University, CNRS, UMR 7281 BIP, Marseille 13000, France
[e] Université de Paris, Institut de physique du globe de Paris, CNRS UMR 7154, Paris cedex 05, 75238, France
[f] Laboratoire de Géologie de Lyon, CNRS-INSU, Lyon I University, 69000 Lyon, France
[g] Cerege, Aix-Marseille University, Aix-en-Provence, France

ABSTRACT

Fougerite, the natural green rust, first discovered in soils and universally considered as responsible for the blue-green colour of gleys and an indicator of reducing conditions, has been recently considered as a key mineral for life's emergence in the alkaline hydrothermal vents theory. It inherits all of the reactive properties of layered double hydroxides in its hydrated interlayer but also the specific reactivity of mixed Fe(II)-Fe(III) compounds, including redox reactivity with metals and metalloids. Along with its structural and compositional analogy with metallo-enzymes, all these properties have stimulated research on the possible role of fougerite as a membrane, and a catalytic engine, especially where gradients of pH, redox potential and temperature favour mixing of chemically contrasted reactants, such as at hydrothermal systems. Although the presence of fougerite, however difficult to detect, has never been reported at alkaline hydrothermal systems, we have thermodynamically evaluated whether the environmental conditions met in such modern oceanic systems are compatible with the formation of fougerite. Data on fluids from the Lost City hydrothermal field (30°N, Mid Atlantic ridge, Seyfried et al. (2015)) support the reducing nature of this environment, close to the lower limit of stability of water at 90 °C and 80 atm. Calculations show that equilibrium with amakinite, the rare ferrous analogue of brucite, is more likely than equilibrium with brucite. This allows for computing *in situ* pH values close to 8 and thus mildly alkaline, while pH measured on board on vent fluids at 25 °C is higher than 10. This is in favour of the occurrence of ferrous hydroxide deeper in the root of the hydrothermal system where temperature is higher and pH are lower compared to seafloor vents where the fluids discharge. Secondary oxidation of amakinite, thanks to the recurrent circulation of seawater in the hydrothermal conduits, will necessarily lead to fougerite formation.

To deepen this question, several lines of investigation are finally proposed, including *e.g.*, the stability of fougerite at elevated temperatures and pressures, its reactivity with key elements for life such as C, N, P, Mo, Ni, S *etc.* and its potential role for free energy conversion and basic functions of metabolism.

1. Introduction

Life relies on free energy sources that all derive from electrochemical tensions driving redox reactions organized in spatially separated compartments. In biota, free energy available in the environmental is converted into chemical energy in the form of high ATP/ADP disequilibria *via* spatially organized chains building up electrostatic membrane potentials which in turn drive phosphorylation (*i.e.*, ATP-generating enzymes). Metalloenzymes play crucial roles in these processes, hence the interest of structural analogies between active sites of these enzymes and specific minerals built up with the same metals and that could have occurred when life emerged on Earth (Williams and Fraústo da Silva, 1997). From this perspective, fougerite is appealing, since it structurally resembles the iron-bearing active sites of several metalloenzymes likely

---

present already in our last common universal ancestor (LUCA), and in particular of the soluble form of methane (CH_4) monooxygenase involved in microbial methane oxidation (Fig. 1) (Nitschke et al., 2013). Fougerite is the naturally occurring mineral featuring the overall structure of green rust, where Fe is present both as Fe(II) and Fe(III) in the octahedral hydroxide layer, where it can partly be substituted by Mg (II) (Trolard et al., 1996, 1997; Trolard and Bourrié, 2008). Fougerite can hence be seen as a partly oxidized member of a solid solution between the ferrous hydroxide amakinite $Fe(OH)_2$ and brucite $Mg(OH)_2$. While brucite is a well-known mineral of common occurrence in alkaline hydrothermal systems, the importance of amakinite is likely underestimated.

Amakinite is a rare mineral on Earth, first characterized in kimberlites, and for which some substitution of iron by magnesium or manganese has been reported (Kozlov and Levshov, 1962; Fleischer, 1962; Sviridov and Yakovlevskaya, 1973; Anthony et al., 1997). Its occurrence has also been reported in oceanic serpentinites drilled below the Lost City alkaline hydrothermal field (Beard et al., 2009; Klein et al., 2009; Boschi et al., 2017), in carbonaceous chondrites (Pignatelli et al., 2016), and in sediments associated with water seeping from a dam, where a tubular hollow structure is considered as a living habitat for iron bacteria (Sun et al., 1995).

Iron and oxygen rich "Poorly-characterized phase" (PCP), a major constituent of carbonaceous chondrites was later identified in the Murchison meteorite belonging to the CM group of carbonaceous chondrites. PCP was associated with a complex intergrowth of cronstedtite and tochilinite $6FeS – 5 Fe(OH)_2$, a regular interstratified mineral composed of alternating mackinawite and brucitic layers (Nakamura and Nakamuta, 1996). In many PCPs, such as those found in the Murchison meteorite, brucitic layer is 100% $Fe(OH)_2$, *i.e.*, amakinite, which means that tochilinite is a regular interstratification of mackinawite and amakinite. Amakinite was also observed in corrosion of steel in hot salt brines between 90 and 200 °C (Nagies and Heusler, 1998).

The potential key role of fougerite has then been brought to the forefront for issues on life's emergence on Earth due to the well-recognized catalytic properties of fougerite in organic and inorganic syntheses and its ion exchange properties (Nitschke and Russell, 2012; Russell, 2018; Branscomb and Russell, 2018a, 2018b). This interest for fougerite is in particular based on its potential presence in alkaline hydrothermal vents (AHV) proposed as a potential locus for the emergence of primordial metabolisms on Earth. It is now increasingly recognized that vent environments may have been intimately connected with life's emergence and evolution as demonstrated by fossils throughout Earth's history (Georgieva et al., 2021). However, fougerite was neither directly identified in chimneys found in alkaline hydrothermal vents nor in the deeper conduits of the hydrothermal systems.

The aims of this paper are then:

1. to describe how fougerite was recently considered as a "must have" mineral in the submarine alkaline hydrothermal vents' hypothesis or the origin of life;
2. to review current knowledge on the structure and properties of fougerite and green rusts that are relevant in this context;
3. to evaluate if the conditions met in modern alkaline hydrothermal systems, *i.e.*, in the Lost City hydrothermal field are compatible with fougerite's domain of stability, considering the substantially different redox conditions of the early Earth;
4. to identify research questions that must be addressed to understand the role of fougerite in the reaction schemes proposed to have contributed to life's emergence on Earth.

2. A putative role of fougerite in the alkaline hydrothermal vent theory for life's emergence

It was recently argued based on thermodynamic arguments (Duval et al., 2020a, 2020b) that the crucial drivers making the emergence of life possible are processes in which *environmental chemical* disequilibria drive metabolic reactions uphill (*i.e.*, promote endergonic reaction networks). From our understanding of extant life, it can be deduced that strong redox and pH gradients were already present in the primordial environments where life emerged.

2.1. Black smokers vs. alkaline vents

Hydrothermal vents on the ocean floor are intriguing due to their capability of furnishing locally very strong and persistent gradients of temperature, elemental concentrations, redox potentials and pH, as a result of the mixing between oxygenated seawater and reduced hydrothermal fluids. These hydrothermal fluids result from continuous and multistage water-rock reactions all along their journey from the recharge zones to the roots of the hydrothermal system (down to about 7 km deep) up to the discharge zones (*i.e.*, the hydrothermal vents) (Andreani et al., 2013; Andreani and Ménez, 2019). Depending on the lithology of the rock with which the water interacts, two types of oceanic vents are commonly distinguished:

1. the basalt-hosted "black smokers" characterized by high temperatures (up to 400 °C) fluids with highly acidic pHs (down to values of 3), and high concentrations of dissolved metals and silica, as well as reduced sulphur species. When discharged in seawater, these reduced fluids cause the precipitation of Fe-Mn-Cu-Zn-Pb sulphides, hence the black colour of the plume and the associated chimney mineralogy found in such hydrothermal vents (Fouquet, 2011);
2. the serpentinite hosted "alkaline vents" characterized by lower temperatures (up to 116 °C) (Seyfried et al., 2015), and higher pHs (around 10). Compared to black smokers, discharged fluids are
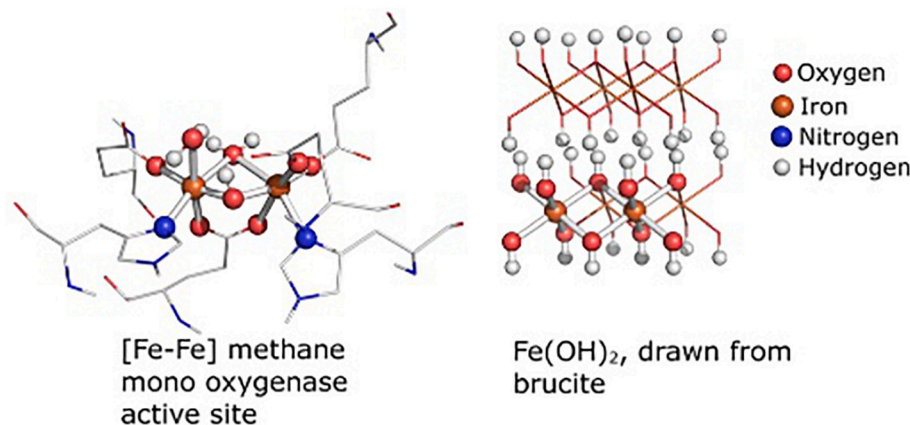

Fig. 1. Structural analogy between the active site of the soluble form of methane monooxygenase and the ferrous hydroxide amakinite (or "ferroan brucite"), a structural component of the brucitic layer of fougerite, a mixed ferrous and ferric hydroxide. A μ_2-OH bond, with 2 OH ligands doubly bridging iron atoms is common to the active site of the enzyme and to amakinite octahedral layer, reproduced from Nitschke et al. (2013)(For interpretation of the colours in this figure, the reader is referred to the web version of this article.)

Oxygen
Iron
Nitrogen
Hydrogen

[Fe-Fe] methane mono oxygenase active site

$Fe(OH)_2$, drawn from brucite

depleted in metals, but enriched in reduced compounds such as hydrogen, methane, and formate, $HCOO^-$. Upon mixing with modern seawater, this alkaline fluid precipitates carbonate-brucite chimneys, hence their whitish colour (Arndt, 2011).

Whereas black smokers are found along fast spreading ridges and derive from interaction with mafic rocks, some alkaline hydrothermal vents such as in the studied site of Lost city result from the interaction of seawater with ultramafic mantle rocks that are enriched in iron compared to basalt (Schwarzenbach and Steele-MacInnis, 2020). The hydration of ferro-magnesian silicates (olivine and pyroxene) found in mantle-derived rocks is a process known as serpentinization, forming mainly serpentine, brucite, and iron oxides in the form of magnetite.

It is postulated that first ferrous hydroxide ("a ferroan brucite" *i.e.*, amakinite, $Fe(OH)_2(cr)$) forms and is secondly oxidized (Beard et al., 2009; Klein et al., 2009; Templeton and Ellison, 2020), hence leading to magnetite formation. The notation $Fe(OH)_2(cr)$ stands for a crystalline solid, while the notation $Fe(OH)_2(ppt)$ designates a precipitate whose crystallinity is not specified; $Fe(OH)_2(am)$ would designate a solid whose amorphous character is specified. Fougerite is likely to form as an intermediate in this process. Goethite, lepidocrocite, haematite, maghemite and magnetite have all been obtained by oxidation of $Fe(OH)_2(ppt)$, with either green rusts or ferrihydrite intermediate compound. Green rusts form when oxidation proceeds slowly with dissolved oxygen input, whereas ferrihydrite forms when oxidation is sudden, as by air entry input (Trolard and Bourrié, 2008).

2.2. Abiotic genesis of amino-acids in alkaline hydrothermal systems

Abiotic hydrocarbons and low molecular weight carboxylic acids were suggested to form abiotically as a consequence of the hydrothermal alteration of mantle derived rocks (Konn et al., 2009). Recently, abiotic amino-acid tryptophan ($C_{11}H_{12}N_2O_2$) was observed in association with Fe-rich saponite, a smectitic clay formed at temperature below 200 °C in deep ultramafic rocks underlying the famous alkaline hydrothermal vents of Lost City (Ménez et al., 2018). It potentially forms from thermodynamically predicted pyruvate ($C_3H_3O_3^-$) and indole (C_8H_7N). Experimentally, pyruvate in the presence of green rusts and ammonia forms the amino-acid alanine $C_3H_7NO_2$ and lactate along with minor acetate CH_3COO^- concentrations, under mild temperature conditions (up to 80 °C) and with redox conditions ranging between pe = 5 and 11 (Barge et al., 2019). The nature of the end product, lactate and/or alanine depends on the oxidation state of the oxyhydroxide used (Barge et al., 2019). This type of reaction observed with Fe-bearing clay minerals suggests they could occur too with layered double hydroxides such as fougerite, often improperly designated as anionic clay minerals.

2.3. Alkaline hydrothermal vent hypothesis for life's emergence

In the submarine alkaline hydrothermal vents hypothesis for life's emergence, the mineral interface between serpentinization derived alkaline hydrothermal fluids and seawater is considered to have provided the conditions required for the emergence of life on Earth (Russell et al., 1989). In these venting systems, occurring at the seafloor, large and self-organized porous mineral structures form as the result of chemical and redox disequilibria in the discharge area where reduced vent fluids mix with mildly oxidized seawater (Barge et al., 2019).

These structures would have consisted of redox-active minerals forming networks of interconnected cavities lined by either inorganic walls or amyloidal membranes (Duval et al., 2020a) within an insulated matrix of other minerals acting as barriers. It has recently been experimentally demonstrated that reduction of CO_2 to formate using H_2 as electron donor does occur in the presence of pH- and redox-gradients corresponding to those of the alkaline hydrothermal vents (Hudson et al., 2020).

It has furthermore been suggested by Duval et al. (2020a) that redox-

reactive and structurally flexible green rust fougerite nanocrystals may have formed electron- and anion-transporting pores within the electrostatic and pH-barriers, possibly emulating the function of life's enzymes that generate phosphate-transfer potentials (driving all metabolic reactions of extant life) and hosting catalytic reactions crucial to early metabolism (Fig. 2).

Mineral barriers may have created and maintained steep ionic disequilibria and fougerite-containing nanoparticles potentially participated in the conversion of environmental redox energy into the chemical disequilibria driving metabolic processes in extant life (Duval et al., 2020a).

We are not sure whether the discussed structures need to be very abundant. It is even conceivable that a single cavity might be enough to spawn life. Oceanic alkaline hydrothermal vents were first discovered in two situations: (i) the Lost City-hydrothermal field, near the Mid-Atlantic Ridge at 30°N (Kelley et al., 2001, 2005) and (ii) in the seafloor of the Eyjafjordur, off the north coast of Iceland (Marteinsson et al., 2001; Russell and Arndt, 2005). Since their present day stability is of several 10,000 years (Früh-Green et al., 2003), there is ample time for trying out all kinds of reaction schemes in the myriad cavities of each chimney. And yes, one might call these structures analogues of prebiotic environments for the synthesis of organic compounds. The ultimate free energy driving all the considered reactions and processes would of course be the combined action of the electrochemical tension (*i.e.*, volts of the barrier) and the pH-gradient (chemical potential).

Although geochemical conditions of the Hadean/Archean ocean as well as global mineralogical composition of underlying rocks should have been different from the modern ones, one can consider Lost-City type alkaline hydrothermal vents as the closest known analogues of AHV of the Archean ocean regarding temperature, pH and redox gradients. They can consequently be used as a proxy of putative prebiotic environments.

The favourable geochemical conditions for such a system are: a pH gradient ranging from values of the primordial ocean (about 5.5 to 6.5) to the ones of alkaline hydrothermal fluids (about 9 to 11) and a temperature gradient between the temperature of the Hadean/Archean ocean and the interior of the alkaline vents (*i.e.*, from 70 °C to 120 °C) (McLeod et al., 1994; Halevy and Bachan, 2017). In the Hadean/Archean ocean, total concentration of Fe^{2+} is supposed to have been of the order of 1 mM (Williams and Fraústo da Silva, 1997), *i.e.*, much more abundant than today. In contact with alkaline vents, Fe^{2+} would have precipitated to form ferrous hydroxide (amakinite) and fougerite.

These conditions were rarely used in experiments and the behaviour of green rusts under such conditions is poorly documented. However, recent works have started to explore experimentally the behaviour and role of green rusts in potential prebiotic environments: in "chemical gardens" (Stone and Goldstein, 2004), in Precambrian oceans, in the genesis of iron formations(Halevy and Bachan, 2017; Halevy et al., 2017), and in experimental analogs of alkaline hydrothermal vents (Barge et al., 2019; Altair et al., 2021). The variety of processes that can be carried out by the different forms of fougerite and green rusts has already been the subject of the review by Usman et al. (2018).

On this basis, it is possible to infer the main interactions between chemical elements and green rusts (Latta et al., 2015) that can be explored in the context of AHV scenarios for the emergence of life (Table 2, Fig. 8).

3. Fougerite and green rusts

3.1. Fougerite as an indicator of reducing conditions in soils

Soil colour has long been closely related to the nature of the iron oxides they contain, more specifically to their degree of hydration, their redox state and their relative abundances (Taylor, 1981; Vysotskii, 1999). Since the early development of soil science, the blue-green colour has been used as characteristic of reducing conditions, a universal
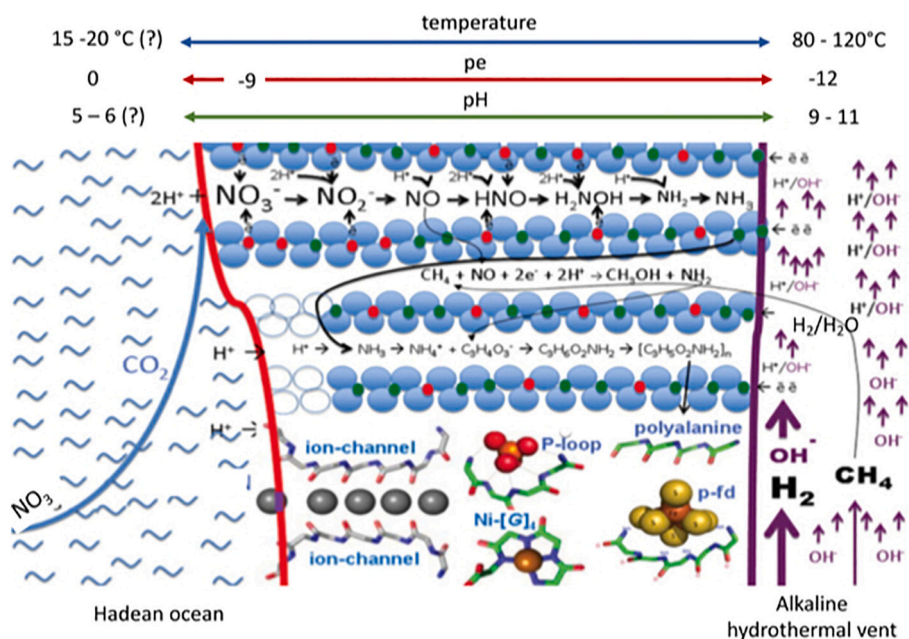
Fig. 2. Interaction fougerite-milieu and resulting reactions in the interlayers in alkaline hydrothermal vents, modified from Russell (2018).

criterion in national soil classifications, *e.g.*, in England and Wales (Avery, 1973), France (Baize and Girard, 2009), the USA (US Soil Survey Staff, 2010) and in the World Reference Base (WRB) proposed by the International Union of Soil Science (IUSS Working Group WRB, 2014). This blue-green colour turns into ochre when iron in soils oxidizes in contact with the oxygenated atmosphere (Vysotskii, 1999). This morphological feature, possibly related to microbial activity, has been attributed to the occurrence of mixed Fe(II)-Fe(III) compounds with a likely, but much debated, green rust structure (Taylor, 1981; Lewis, 1997).

Fe-bearing green rust, now homologated as fougerite, was first observed in 1996 in the Fougère's forest (Brittany, France) in soils developed on a granitic arena under temperate oceanic climate (Trolard et al., 1996, 1997). It was then approved as a new mineral named fougerite by the International Mineralogical Association under number 2003–57 (Trolard et al., 2007).

The following conditions in these blue-green soils are necessary for the presence of fougerite (Trolard and Bourrié, 2008):

- an excess of water;
- limited oxygen sources;
- the presence of bio-available substrates (carbon sources);
- temperature conditions favourable to microbial activity;
- the presence of Fe, that can record more or less irreversibly the variations in aerobic / anaerobic conditions.

Beyond the site of Fougères in France, fougerite has rarely been directly identified in natural environments because of its small abundance, large reactivity and poor stability under an oxygenated atmosphere. However, minerals described in five other contexts can be ascribed to fougerite: (i) 4 mm below the surface of ochreous sediments in the drainage system of an abandoned coal mine (South Wales, UK) (Bearcock et al., 2006); (ii) in groundwater collected from an artesian well in a chalk aquifer or associated with deep fractures in an underground granite tunnel (Denmark) (Christiansen et al., 2009); (iii) close to the iron redoxcline of the ferruginous Matano Lake (Indonesia) with persistence in the water column and sediments (Zegeye et al., 2012); (iv) in CO₂-rich soils associated with gas discharge (mofettes) during final stages of volcanic activity (Czech Republic) (Rennert et al., 2012); (v) at the subsurface oxic/anoxic interface in a metal-polluted uranium mine

drainage (Thuringia, Germany) (Johnson et al., 2014). The presence of fougerite was also suspected in anoxic sediments drilled in the Marmara Sea: upon core retrieval, the blue-greenish colour of the sediment turned to ochre upon contact with the oxygenated atmosphere (Pierre Henry, CNRS, Aix-en-Provence, personal communication).

3.2. Green rusts as intermediate Fe(II)-Fe(III) hydroxides

As early as 1935, in an iron bar corrosion experiment, transitional blue-green compounds were observed during the progressive oxidation of Fe(0) (Girard and Chaudron, 1935). In steel corrosion, green rusts have been identified as intermediate products (Stampfl, 1969; McGill et al., 1976; Fonseca et al., 1998; Refait et al., 1998a,b). Their variable structure was characterized by solid state physics, and their stability was delimited using classical Pourbaix diagrams (*Eh*, pH), or equivalently (pe, pH) diagrams; pe is defined (Sillén, 1967) as:

$$pe = -log\{e-\}, \tag{1}$$

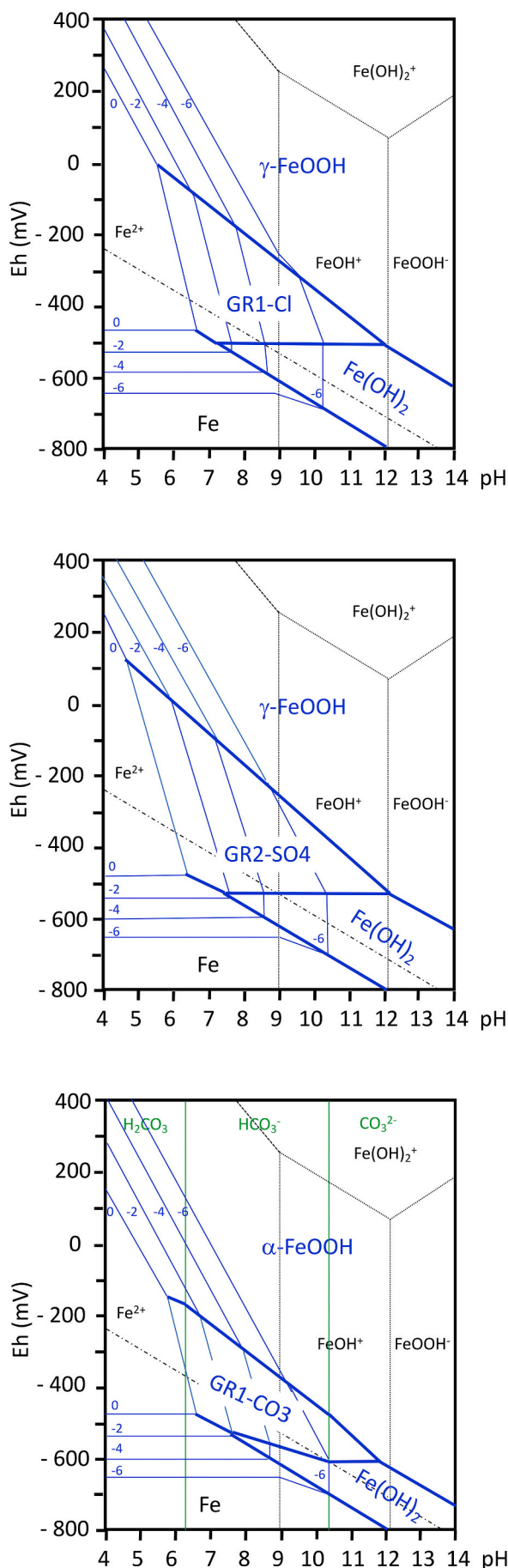in which {e-} is the activity of the electron, and related to the redox potential *Eh* by:

$$pe = FEh/(ln10)RT, \tag{2}$$

where *F* is the Faraday constant and *R* the molar gas constant.

Corrosion studies represent therefore a large corpus of green rusts' thermodynamic and structural data (Misawa, 1973; Refait and Génin, 1993; Drissi et al., 1995; Hansen and Koch, 1998; Refait et al., 1999). Pourbaix diagrams of chloride-, sulphate- and carbonate- green rusts are given below (Fig. 3) in standard temperature and pressure conditions, in pure chloride, sulphate or carbonate systems (Génin et al., 1998). Note that green rusts / amakinite (Fe(OH)₂) transition occurs under alkaline and reducing conditions, just above the reduction of sulphate into sulphide.

3.3. Mineralogical structures of green rusts

Green rusts, including fougerite, belong to the larger family of the layered double hydroxide minerals, which consist of sequences of stacked layers of edge-sharing hydroxide octahedra (the so-called "brucitic layer"). All octahedral sites of the brucitic layers are

occupied by both divalent and trivalent metal ions (Allada et al., 2002; Sparks, 2003). The presence of trivalent ions in the octahedral layer generates an excess positive charge per formula unit, which is fully balanced by the negative charges carried by the interlayer anions A^{-n}.

Layered double hydroxides' general structural formula can accordingly be written as: $[M(II)_{1-x} M(III)_x (OH)_2][x/n\ A^{-n} \cdot m\ H_2O]$, in which M(II) can be Ca, Mg, Ni, Co, Zn, Mn and Fe while M(III) can be Al, Fe and Cr (Sparks, 2003). The interlayered anions can include hydroxyl OH^-, chloride Cl^-, bromide Br^-, iodide I^-, nitrate NO_3^-, perchlorate ClO_4^-, carbonate CO_3^{2-}, sulphate SO_4^{2-}, selenate SeO_4^{2-}, oxalate $C_2O_4^{2-}$ as well as lactate CH_3–CHOH–COO^- (Fig. 4). The interlayers are hydrated.

In addition to fougerite, minerals with a layered double hydroxide structure include pyroaurite (with Mg(II) and Fe(III) in the brucitic layer, and CO_3^{2-} in the interlayer), iowaite (Mg(II), Fe(III); Cl^-), hydrotalcite (Mg(II), Al(III); CO_3^{2-}) and meixnerite (Mg(II), Al(III); OH^-) (Trolard and Bourrié, 2008). The fact that layered double hydroxides can accommodate different metals in their brucitic layer as well as different anions and variable water content in the interlayer makes them extraordinarily reactive and results in numerous studies addressing their catalytic activity (Trolard and Bourrié, 2008, 2012).

Bernal et al. (1959) proposed models for the green rusts' structure (Fig. 4), which were subsequently refined by many other scientists worldwide.

They distinguished two structures for these iron-bearing layered double hydroxides for which Me(II) = Fe(II) and Me(III) = Fe(III): GR1 in which the anions are spherical (*e.g.*, Cl^-) or planar (*e.g.*, CO_3^{2-}) (Fig. 4a) and GR2 where interlayer anions such as SO_4^{2-} have a three dimensional structure (Fig. 4b). Accordingly, the unit cell dimension *c*, defined as the distance between layers, is larger in GR2 than in GR1. Two water layers are also present in GR2 but only one in GR1 (Trolard and Bourrié, 2012).

3.4. Specificity of the fougerite mineral from Fougères

Fougerite is sparse in soils (total Fe_2O_3 content is only *ca.* 4 wt%) and thus difficult to analyze in soil matrix. When analyzed with X-ray diffraction, its main peak is very close to the main peak of kaolinite, which is widespread and more abundant. With particle sizes less than 500 nm (Trolard, 2006), this labile nanomineral cannot be separated from other minerals (Feder et al., 2018). Its structure was nonetheless characterized by X-ray absorption spectroscopy (XAS) (Refait et al., 2001), Raman spectroscopy (Trolard et al., 1997), as well as Mössbauer spectroscopy carried out both in the laboratory (Génin et al., 1998) and *in situ* in the field (Feder et al., 2005). Its characteristic texture was also highlighted using scanning electron microscopy (Trolard et al., 2007). In natural fougerite, Mg(II) substitutes partly for Fe(II). Evidence for the presence of Mg in the brucitic layer is supported by the XAS radial distribution obtained for fougerite, which is an intermediate between the ones obtained for GR1 and for synthetic pyroaurite, *i.e.*, between Fe(II)-Fe(III) and Mg(II)-Fe(III) hydroxy-carbonates (Refait et al., 2001). Fougerite stacking sequence type is GR1 (Fig. 4a) and the structure of this ternary compound can be described by the general formula: $[(Fe(II), Mg(II))_{1-x} Fe(III)_x (OH)_2]^{+x} [x/n\ A^{-n} \cdot m\ H_2O]^{-x}$.

The nature of the interlayer anion is relevant with respect to mass balances of anions, *e.g.*, chloride as discussed below with respect to chloride-green rust *versus* iowaite formation, or carbonate, as carbonates

(caption on next column)
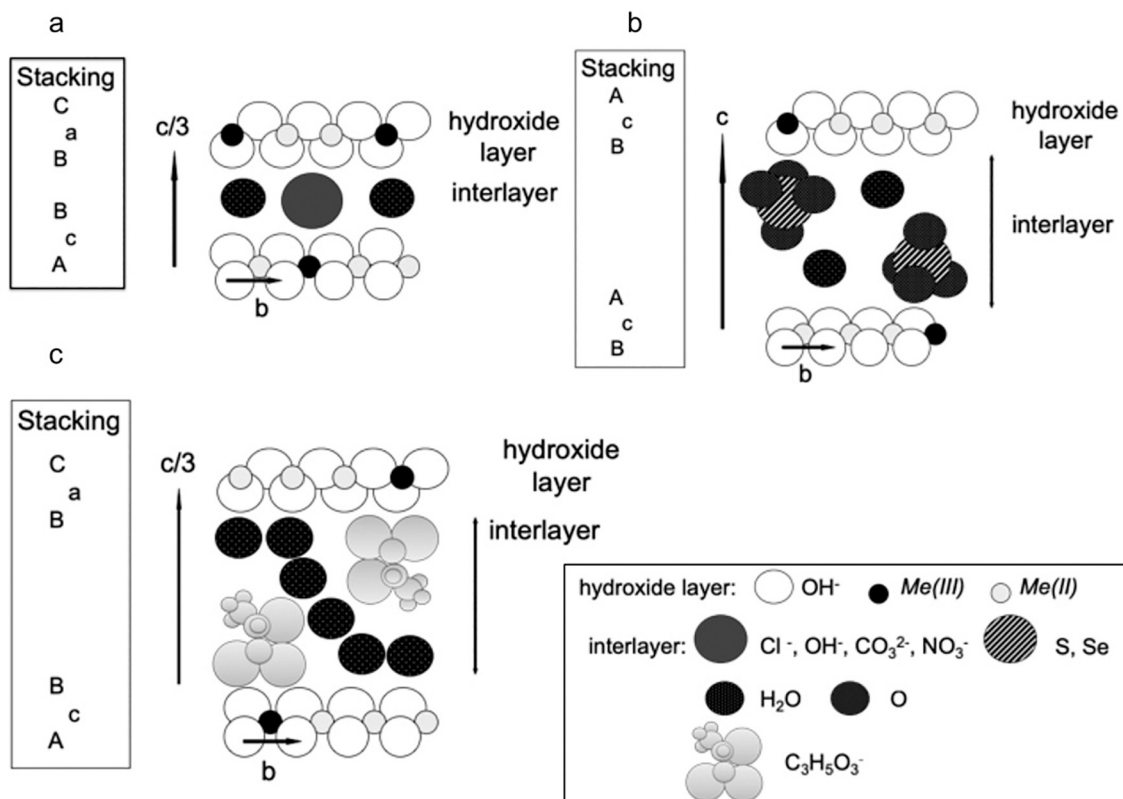
Fig. 4. Stacking sequences and structures of layered double hydroxides (modified from Trolard and Bourrié (2012) and Sabot et al. (2007). For green rusts, M(II) = Fe(II) and M(III) = Fe(III); Panel (a) corresponds to GR1 structure, panel (b) to GR2 structure and panel (c) to GR-lactate structure; Note that only the main interlayer anions are shown in the drawings of the structure; *a*, *b* and *c* correspond to unit cell dimensions; in the inserts with stacking, A, B and C correspond to OH planes, a, and c correspond to planes of octahedral sites.

are present in some hydrothermal environments. However, this results only in very small variations in the interlayer distance. Thorough fitting of X-ray diffractograms gives a value of 2.375 nm for the unit cell dimension *c* (Trolard and Bourrié, 2008), which favours OH^- as the interlayer anion (Trolard and Bourrié, 2012), in the fougerite from Fougères instead of CO_3^{2-}, as proposed in some studies (Génin et al., 2005). If CO_3^{2-} was the interlayer anion in fougerite from Fougères, *c* would be in the range 2.25 nm to 2.28 nm (Trolard and Bourrié, 2008). In addition, the soil solution of Fougères shows pH values of *ca.* 7, at which CO_3^{2-} concentrations are too small to allow for equilibrium between a carbonate GR (GR1-CO3) and the soil solution. Under these pH conditions, a mixture of hydrogeno-carbonate and carbonate ions can be theoretically present in the fougerite interlayers but in Fougères, soil solutions are undersaturated with respect to (HCO_3^-/CO_3^{2-})-green rust, while they are always oversaturated with respect to hydroxyl-bearing green rust (GR-OH). Moreover, when fougerite oxidizes, it transforms into lepidocrocite, an oxyhydroxide that cannot form in the presence of carbonate ions (Schwertmann and Fechter, 1994).

This does not preclude the possible formation of carbonate-fougerite under neutral to alkaline and reduced conditions or of chloride- or sulphate- fougerite under saline and reduced conditions.

3.5. Domains of composition and thermodynamic data of green rusts and fougerite

3.5.1. Domain of composition of fougerite and green rusts

Green rusts are characterized by a variable Fe(III)/Fe$_{total}$ ratio ranging between 1/4 and 1/3, as determined by Mössbauer spectroscopy (Cornell and Schwertmann, 2003), supported by XAS investigations (Refait et al., 2001), and constrained by structural considerations (Trolard et al., 2007). Larger ranges of Fe(III)/Fe$_{total}$

ratios have been experimentally observed, but they are related to changes in the crystal structure occurring when Fe(III) occupies neighbouring octahedra. This comes with a violation of Vucelič's rule, however compensated by a loss of protons by some of the structural OH forming the brucitic layer (Génin et al., 2005). This corresponds to an oxolation process, forming Fe-O-Fe bonds instead of Fe-OH-Fe bonds (Jolivet, 2000; Bourrié et al., 2004), and leads to iron protooxyhydroxides, that are precursors of lepidocrocite and haematite, but do not strictly correspond to green rusts.

Similarly, the compositional stability domain of the fougerite from Fougères (Fig. 5) has been constrained by Mössbauer spectroscopy, electron microprobe analyses, and by taking into account the Vucelič's rule and the fougerite solubility (Trolard et al., 2007). The range of Fe (III)/Fe$_{total}$ ratio, spanning from 1/4 to 2/3, is given by Mössbauer spectroscopy; the Fe(III)/(Fe(II) + Mg) mole ratio cannot be smaller than 1/4 as both ferrous hydroxide and magnesium hydroxide are highly soluble and a minimum number of Fe(III) ions in the brucitic layers is necessary to stabilize the structure. Conversely, this ratio must not be larger than 2/3 for each Fe(III) ion to be surrounded by divalent cations in the brucitic layer. The Mg(II)/Fe$_{total}$ mole ratio is given by electron microprobe analyses and ranges from 0.18 to 0.62.

3.5.2. Gibbs free energies of formation of green rusts and fougerite

Thermodynamic properties of minerals mainly depend on their chemical composition, and to a lesser extent on their structure. For layered double hydroxides and particularly for isostructural green rusts and fougerite that show very limited variation in their brucitic layer composition, thermodynamic properties can be related to the electronegativity of the interlayer anions (Bourrié et al., 2004).

The partial charge model (Jolivet et al., 1994) was used to establish the relationship between the Gibbs free energy of formation $\Delta_f G_m^{\circ -}$ of
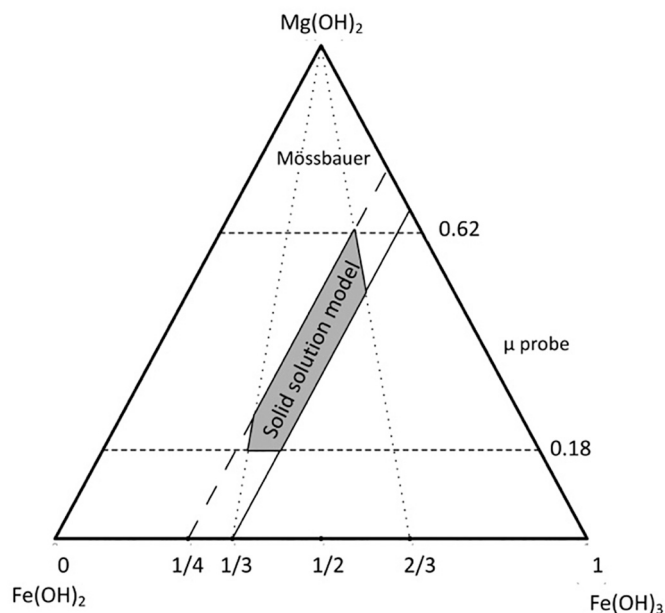
Fig. 5. Composition stability domain of fougerite from Fougères (in grey) from Trolard et al. (2007). It is derived from a solid solution model (shown with solid and long dashed lines) constrained by Fe(III)/Fe$_{total}$ ratio comprised between 1/4 and 1/3, the Mg/Fe$_{total}$ mole ratio comprised between 0.18 and 0.62, and the Fe(III)/(Fe$_{total}$ + Mg) mole ratio determined by electron microprobe analysis (μ−probe: short dashed lines) and Mössbauer spectroscopy (dotted lines).
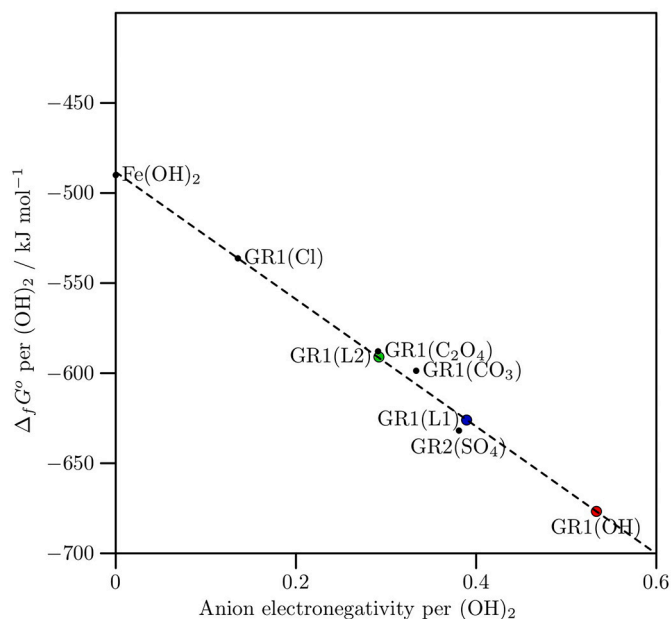
Fig. 6. Relationship between Gibbs free energies of formation of green rusts and fougerite as a function of electronegativity of the interlayer anion. Filled black circles: measured values used to compute the linear regression, from Ben Nacib et al. (2016); red filled circle: estimated value for GR1-OH; blue and green filled circles: estimated values for GR1-lactate for the two structural formulas GR1-L1 and GR1-L2, from Sabot et al. (2007). (For interpretation of the references to colour in this figure legend, the reader is referred to the web version of this article.)

green rusts and fougerite and the Allred and Rochow's electronegativity of the interlayer anions, whatever their structure (*i.e.*, GR1 or GR2) (Fig. 6, eq. 3) (Ben Nacib et al., 2016):

$$\Delta_f G_m^{°-}/n = -488.354 - 353.11\chi/n, r = -0.994, N = 5, \qquad (3)$$

where the Gibbs free energy of formation of the mineral, $\Delta_f G_m^{°-}$, is in kJmol^{-1}, n is the number of (OH)$_2$ in the mole formula, and χ the electronegativity of the considered anion; r is the coefficient of correlation and N is the number of samples. Anion exchange is possible in the hydrated interlayer and the stability follows the sequence: $Cl^- < C_2O_4^{2-} < CO_3^{2-} < SO_4^{2-}$. This makes it possible to estimate the Gibbs free energies of formation of fougerite with hydroxide as interlayer as in Fougères, Brittany (GR1-OH) and of lactate green rust for which thermodynamic data are lacking (Table 1).

3.6. Syntheses of green rusts

3.6.1. Abiotic syntheses

Green rusts can be easily synthesized (Murad, 1990) and several laboratory approaches have been used for this purpose, as recently reviewed by Bhave and Shejwalkar (2017). The most frequently used protocol is the co-precipitation of ferrous and ferric salts and the joint oxidation of ferrous salts. Electrolytic oxidation of an iron anode under controlled conditions is much less used. Whatever the protocol, all detailed below, syntheses are made at room temperature (20 °C to 25 °C) and atmospheric pressure (1 atm). In the co-precipitation method, green rust at the proper oxidation state is obtained by mixing stoichiometric amounts of ferrous and ferric salts with continuous stirring under an O$_2$-free atmosphere. The final Fe(III)/Fe$_{total}$ ratio in green rust can be controlled by the concentrations of the precursor salts, which can be Fe(II)-sulphate combined with either Fe(III)-nitrate or Fe(III)-chloride. Fe(III)-sulphate can also serve as a ferric precursor in the synthesis of green rust (Géhin et al., 2002). Green rusts can also be obtained by partial oxidation of ferrous salts under controlled anaerobic conditions. In that case, the Fe(II) salt solution is mixed with sodium hydroxide, hence leading to the precipitation of Fe(II)-hydroxide (the so-called"white rust") (Stone and Goldstein, 2004). Then the Fe(II)-hydroxide is slowly oxidized through stirring under air. Oxidation is stopped by covering the experimental device when the white colour of Fe(II)-hydroxide turns to greenish-blue, the characteristic colour of green rust. In this approach, melanterite (FeSO$_4$·7H$_2$O) can be used as the starting ferrous salt to form GR2-SO4 (Génin et al., 1996), and FeCl$_2$·4H$_2$O can be used as the precursor salt of GR1-Cl (Génin et al., 1998) respectively. Note that dioxygen is not always necessary for the oxidation of ferrous salt: sodium nitrite, NaNO$_2$ (Hansen et al., 1994a) or sodium nitrate, NaNO$_3$, can also be used to synthesize green rusts (Hansen and Koch, 1998). For synthetic green rusts that do not directly form, anion exchange is used. This is the case of green rusts containing interlayered carbonate or oxalate, because these ions inhibit the formation of the Fe(OH)$_2$ precipitate. GR1-CO3 or GR1-oxalate are then obtained in two steps, first by forming GR2-SO4, then by exchanging the sulphate with carbonate or oxalate ions (Drissi et al., 1994; Refait et al., 1998b).

Table 1
Thermodynamic data used to compute the regression with electronegativity of the interlayer anion (eq. 3) and to estimate the Gibbs free energies of formation of hydroxide-fougerite (GR1-OH) and synthetic lactate-green rust (GR1-lactate).

Mineral	n	χ	$\Delta_f G_m^{°-}$	χ/n
Amakinite Fe(OH)$_2$(cr)	1	0	−490.035	0
GR2-SO4	6	2.286	−631.872	0.381
GR1-Cl	4	0.542	−536.243	0.137
GR1-CO3	6	2.001	−598.661	0.335
GR1-oxalate	8	2.329	−587.873	0.291
Fougerite-OH	3	1.601	−676.74[a]	0.534
GR1-lactate	6	2.337	−625.86[b]	0.389
GR1-lactate	8	2.337	−591.50[b]	0.292

n is the number of (OH)$_2$ groups in the mole formula, *i.e.*, in the layer;
(a) estimated using eq.3, for fougerite as Fe(OH)$_{7/3}$ from Ben Nacib et al. (2016);
(b) estimated using eq.3, for GR-lactate formulas from Sabot et al. (2007).

3.6.2. Biotic syntheses

Green rusts can also be obtained by microbial reduction of Fe(III) oxides carried out in particular by dissimilatory iron reducing bacteria, *i. e.,* bacteria that use iron as terminal electron acceptor for their respiration. Among them, *Shewanella putrefaciens* produces green rusts from the bioreduction of ferrihydrite or lepidocrocite (Fredrickson et al., 1998; Kukkadapu et al., 2006; Parmar et al., 2001; Glasauer et al., 2002; Ona-Nguema et al., 2002; Zegeye et al., 2005). Bio-reduction of a well crystallized lepidocrocite (γ-FeOOH) to carbonate-green rust (GR1-CO3) was in particular investigated in batch cultures of *S. putrefaciens* strain CIP 8040 at 25 °C, an initial pH of 7.5, and using a carbonate ion buffer. Formate was used as the electron donor and experiments were performed without phosphate and in the presence or absence of anthraquinone-2,6-disulphonate as electron shuttle to accelerate or not green rust formation kinetics. When all the starting lepidocrocite is consumed by bacterial respiration, green rust is the major final product, representing 55 to 86% of the solid products (Ona-Nguema et al., 2002). However, when the bacterial Fe(III) reduction does not reach completion (*e.g.,* due to a lack of electron donor), the remaining lepidocrocite induces the transformation of green rust into magnetite (Ona-Nguema et al., 2002). Alternatively, lepidocrocite can be microbially reduced into sulphate-green rust if sulphate is added to the culture medium (Zegeye et al., 2005).

Magnetite can be partially reduced by *S. putrefaciens* using molecular hydrogen, H_2, as electron donor. In that case, Fe^{2+} released by magnetite dissolution precipitates into green rusts and siderite, Fe(*II*)CO₃, (Etique et al., 2016). Note finally that *Dechlorosoma suillum* also produces green rusts through anaerobic bio-oxidation of Fe(II) (Chaudhuri et al., 2001).

3.7. Intercalation properties and reactivity

Chloride (Refait et al., 1998a; Peulon et al., 2003, 2007), sulphate (Misawa, 1973; Géhin et al., 2002; Ruby et al., 2003; Peulon et al., 2003) and carbonate (Drissi et al., 1995; Legrand et al., 2001; Ona-Nguema et al., 2002) are commonly incorporated as interlayer anions in synthetic green rust products, but also possible, yet more unusual, is the intercalation of fluoride (Choi and Batchelor, 2008), selenite (Refait et al., 2000), lactate (Sabot et al., 2007), oxalate (Refait et al., 1998b) and even of larger monovalent aliphatic carboxylate anions, CX (Ayala-Luis et al., 2010).

The basal spacing distance *c* of CX-green rust increases with the length of CX (*i.e.,* with the number of aliphatic chain carbons): 2.68 nm for GR-C9, 2.94 nm for GR-C10, 3.59 nm for GR-C12 and 4.16 nm for GR-C14 (Ayala-Luis et al., 2010). Recent work has shown that synthetic green rusts can also be obtained with interlayered benzene sulphonate, BzS, from GR2-SO4 by ion exchange with sulphate, although the exchange extension is limited (around 18% of intercalation) (Perez et al., 2018) (Fig. 7).

The high reactivity of green rusts and ease of their synthesis together with the biocompatibility of potentially precursor iron oxides make green rusts appealing for environmental (bio)remediation purposes. As many layered double hydroxides, green rusts have been shown to be highly effective for the remediation of environments polluted by a large diversity of metals and metalloids (*e.g.,* Cu, Hg, Ag, Au, Cr and As) (Table 2), as well as organic pollutants (Bhave and Shejwalkar, 2017) (Fig. 8).

These metals and metalloids can have multiple oxidation states in surface and subsurface environments and can interact with the redox active Fe carried by green rusts. These variable oxidation states are associated with variable metal solubility and toxicity. As an illustration, aqueous solutions of silver acetate, as well as silver, gold or copper chlorides were mixed with hydroxy-sulphate green rust suspensions (O'Loughlin et al., 2003b). Ag(I), Au(III) and Cu(II) were readily reduced to Ag(0), Au(0), Cu(0), respectively, that precipitate as nanoparticles (O'Loughlin et al., 2003b). In all cases, magnetite was the product of concomitant green rust oxidation. Metals precipitate as nanoparticles multiply-twinned bearing the same local environment as pure metal phases, as evidenced by XANES and EXAFS (O'Loughlin et al., 2003b).

The reactivity of sulphate-green rust (GR2-SO4) or chloride-green rust (GR1-Cl) with regard to toxic Cr(VI) was also studied. A rapid and complete reduction of Cr(VI) into less soluble and less toxic Cr(III) was observed (Loyaux-Lawniczak et al., 1999, 2000), which further underlines the lack of influence of the nature of the interlayer anion on the overall reaction. By incorporating the metal in the green rust structure, these reactions immobilize the pollutant initially present in the form of dissolved ions. However, an increase of metal mobility may also occur following interactions with green rusts. For example, the reduction of Hg
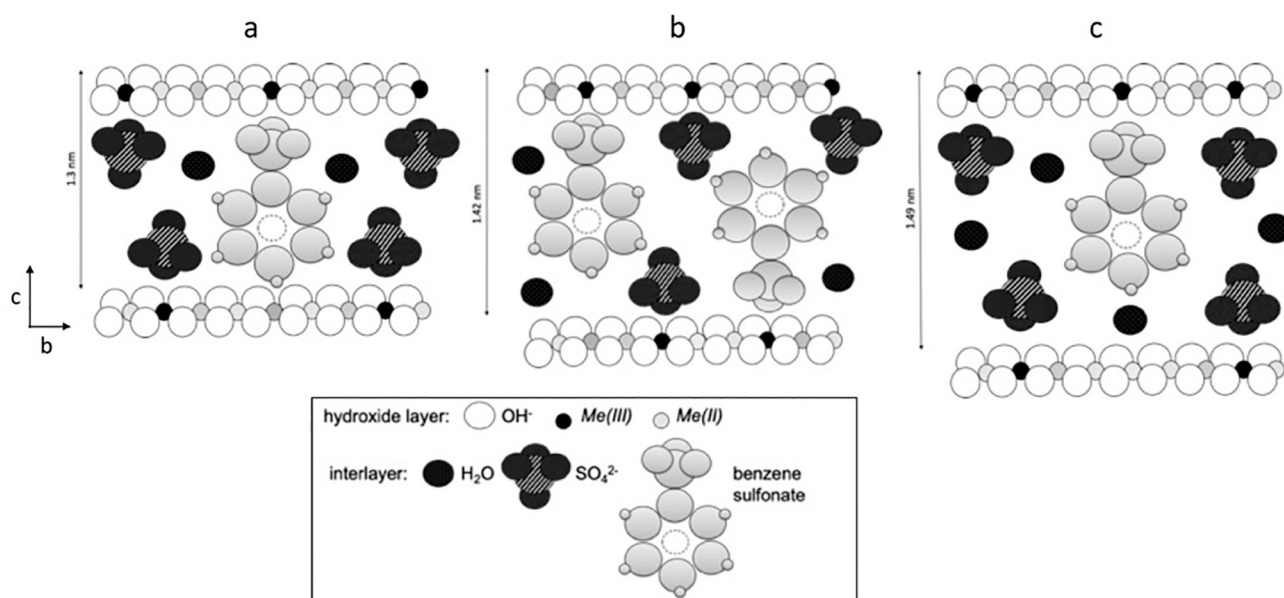

Fig. 7. Possible interlayer arrangement of benzene sulfonate (BzS) in the green rust structure. Calculated basal spacing is shown for each structure: (a) monolayer with dehydrated BzS in a single direction; (b) monolayer with dehydrated BzS moieties facing away from each other and (c) monolayer with hydrated BzS in a single direction, modified from Perez et al. (2018).

Table 2
Reactive elements towards green rusts and types of reactions (modified from (Latta et al., 2015)). Ox. = Conventional oxidation number.

Element	Species	Ox.	Interaction with green rust	References
H	H^+	+i	Structural Protonation/ deprotonation	Bernal et al. (1959) Guilbaud et al. (2013); Ruby et al. (2006)
C	CO_3^{2-}	+IV	Structural interlayer anion	Taylor and McKenzie (1980)
	Oxalate, Lactate,	to	Redox reaction	Lee and Batchelor (2002)
	C9 to C14	-I	Redox reaction	Erbs et al. (1999); O'Loughlin and Burris (2004); O'Loughlin et al. (2010); Sabot et al. (2007)
N	NO_3^-, NO_2^-	+V, +III	Reduction to ammonium	Hansen et al. (1994a, 1996); Larese-Casanova and Scherer (2008); Trolard and Bourrié (1999)
	NH_4^+	-III	Incorporation	Etique et al. (2014); Guerbois et al. (2014); Hansen et al. (1994a); Pankte et al. (2011)
O	OH^-	-II	Structural	Bernal et al. (1959); Bourrié et al. (2004)
F	F^-	-I	Structural interlayer anion	Choi and Batchelor (2008)
Na, K	Na^+, K^+	+I	Interlayer incorporation	Christiansen et al. (2009, 2014)
Mg	Mg^{2+}	+II	Structural in the brucitic layer	Bourrié et al. (2004); Refait et al. (2001)
Al	Al^{3+}	+III	Structural in the brucitic layer	Aissa et al. (2004); Taylor and McKenzie (1980)
Si	SiO_3H^-	+IV	Adsorption, dehydration and silicification of the interlayer	Larese-Casanova and Scherer (2008); O'Loughlin et al. (2010); Ruby et al. (2006); Trolard and Bourrié (2012)
P	PO_4H^{2-}	+V	Adsorption Interlayer incorporation,	Bocher et al. (2004)
	PO_4H^{2-}	+V	green rust stabilization, transformation to vivianite	Hansen and Poulsen (1999); Kukkadapu et al. (2006); O'Loughlin et al. (2010)
S	SO_4^{2-}	+VI	Structural interlayer anion	Refait et al. (1999)
	SO_3^{2-}	+IV	Structural interlayer anion	Simon et al. (1997)
Cl	Cl^-	-I	Structural interlayer anion	Refait et al. (1998a)
	ClO_3^-	+V	Reduction to chloride	Zhang et al. (2021)
	ClO_4^-	+VII	Structural interlayer anion	Aguirre et al. (2020)
Cr	CrO_4^{2-}	+VI	Adsorption, redox reaction	Williams and Scherer (2001)
	Cr^{3+}	+III	Incorporation	Bond and Fendorf (2003); Loyaux-Lawniczak et al. (1999, 2000)
Fe	Fe^{2+}, Fe^{3+}	+II, +III	Structural in the brucitic layer	Bernal et al. (1959)
Co, Ni	Co^{2+}, Ni^{2+}	+II	Structural in the brucitic layer	Hansen et al. (1994b); Parmar et al. (2001); Roh et al. (2000)
Se	SeO_4^{2-}	+VI	Interlayer incorporation	Myneni et al. (1997); Refait et al. (2000)
	SeO_3^{2-}	+IV	Redox reaction	Schellenger and Larese-Casanova (2013)
	Se	0	Transformation to FeSe	Johnson and Bullen (2003)
Br	Br^-	-I		Aguirre et al. (2020)

Table 2 (continued)

Element	Species	Ox.	Interaction with green rust	References
			Structural interlayer anion	
Mo	MoO_4^{2-}	+VI	Adsorption	O'Loughlin et al. (2010)
U	UO_4^{2-}	+VI	Reduction to U(IV)	O'Loughlin et al. (2003a)

(II) to Hg(0) by green rusts increases the overall mobility of mercury, that is then dispersed in the environment, as the release of Hg(0) vapor to the atmosphere represents a significant component of the global mercury cycle (Stein et al., 1996; Schlüter, 2000).

Other experiments, performed in the presence of green rusts, showed that these Fe-bearing layered double hydroxides have also the capability to reduce nitrate into ammonium (Hansen et al., 1996), chlorate into chloride (Zhang et al., 2021), Se(VI) to Se(IV) and Se(0) (Myneni et al., 1997), and U(VI) to U(IV), forming nanoparticles of UO_2 (O'Loughlin et al., 2003a). In addition, chlorinated methane and ethene (Maithreepala and Doong, 2005), or carbon tetrachloride (Erbs et al., 1999) can be dechlorinated by green rusts.

4. On the possible occurrence of fougerite at the Lost City hydrothermal system

To evaluate if the environmental conditions met in modern oceanic alkaline hydrothermal systems are compatible with the formation of fougerite, we have used recent data collected by Seyfried et al. (2015) on fluids of the Lost City hydrothermal field, the best known example of active oceanic alkaline hydrothermal system related to serpentinization.

4.1. Field data on Lost City hydrothermal fluids

In an attempt to augment existing dataset on the chemistry of fluids venting at Lost City (Allen and Seyfried, 2003; Kelley et al., 2005; Ludwig et al., 2006; Proskurowski et al., 2008a, 2008b; Foustoukos et al., 2008; Konn et al., 2009; Lang et al., 2010, 2012) and to better understand the dynamic feedback between mineral alteration and changes in fluid chemistry associated with such hydrothermal system, Seyfried et al. (2015) have recently investigated fluids collected at two vent structures: Beehive (BH) where the fluid flow was vigorous and temperature from *ca.* 91 °C to 116 °C and M6, where fluid escaped more diffusively and temperature was lower *ca.* 53 °C to 78 °C. While ongoing serpentinization occurring at Lost City could have suggested equilibrium with a serpentine - brucite assemblage, the pH values and high silica concentrations measured in these fluids support equilibria with a serpentine (chrysotile) – diopside – tremolite assemblage in the temperature range of 75 °C to 116 °C. The equilibrium shift away from brucite into the tremolite stability field can be explained by ubiquitous gabbroic intrusions in the ultramafic lithosphere underlying the Lost City alkaline hydrothermal field. Seyfried et al. (2015) report relatively small concentrations of chloride, 540 mmol/kg to 550 mmol/kg, *i.e.*, 10 mmol/kg to 15 mmol/kg below that of bottom seawater, attributed either to the incorporation of Cl^- in the serpentine structure in a iowaite component — $[Mg_6Fe(III)_2(OH)_{16}][Cl_2·H_2O]$, a natural layered double hydroxide belonging to the same group as fougerite — or to a dilution effect due to water release associated with dehydration of brucite.

Concerning iron analyses Seyfried et al. (2015) considered that they may incorporate colloidal iron oxides, so that they could not be confidently used to compute Fe speciation in aqueous solution and to check whether Fe speciation was controlled by chemical equilibria with iron oxides. However, their hydrothermal fluid analyses also show elevated concentrations of methane, hydrogen and hydrogen sulphide (H_2S). Accordingly, the presence of Fe(III) and the formation of iowaite, in which iron is exclusively present as Fe(III) is unlikely, unless mixing
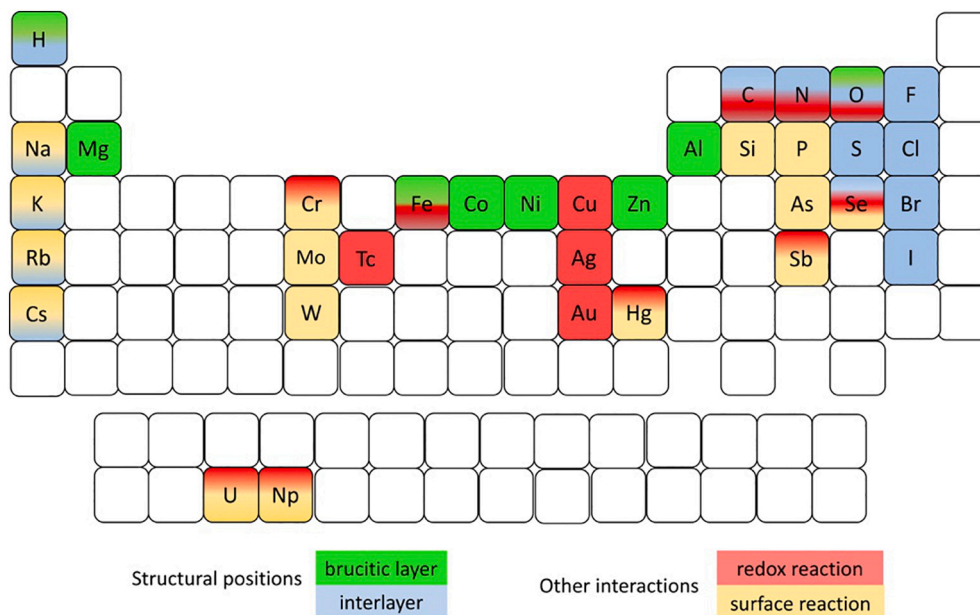
Fig. 8. Periodic table illustrating the possible interactions between green rusts and 34 elements through redox and surface reactions or surface exchange reactions, modified from Latta et al. (2015). (For interpretation of the references to colour in this figure legend, the reader is referred to the web version of this article.)

with oxygenated seawater occurs. Considering that the structure of fougerite consists of Fe(II)-Fe(III) and Mg(II) bearing brucitic layers, it is thus relevant to check equilibria between Lost City hydrothermal fluids and the two end members of the fougerite solid solution, namely brucite, $Mg(OH)_2$, and its ferrous equivalent $Fe(OH)_2$, known as amakinite, whose occurrence was reported in the basement underlying the Lost City hydrothermal field (Beard et al., 2009).

4.2. Equilibrium calculations on Lost City hydrothermal fluids

With this aim to establish fougerite, brucite and amakinite stability fields at Lost City, it was necessary to first evaluate thermodynamic data for aqueous iron as well as the stability of water in such environments.

4.2.1. Thermodynamic data for aqueous iron in line with the specific interaction theory

On the basis of the most comprehensive critical evaluation of iron thermodynamic data (Lemire et al., 2013), Ben Nacib et al. (2016) have recently reevaluated the equilibrium constants for the different forms of aqueous Fe(II) and the Gibbs free energies of formation of green rusts and fougerite. In their critical evaluation, Lemire et al. (2013) used the Specific Interaction Theory (SIT) to extrapolate experimental data to zero ionic strength and provided parameters for the specific interactions between cations and anions in solution. For sake of consistency, as underlined by Lemire et al. (2013), it is better to use the SIT instead of Debye-Hückel extended law or Pitzer's model to compute activity coefficients of solutes and speciation in solution. The SIT database, sit.dat, incorporates specific interaction parameters in addition to equilibrium constants. In the present work, the recently re-evaluated set of equilibrium constants for Fe(II) and Fe(III) species and $\Delta_f G_m^{\circ-}$ of green rusts and fougerite (Ben Nacib et al., 2016), incorporated in a modified version of the SIT database, was used together with PHREEQC software allowing for pH-redox equilibria calculations (Parkhurst and Appelo, 2013).

4.2.2. Stability domain of water at high temperatures and pressures

Calculations shown in section 4.3 were made using the sit.dat database as mentioned before at the temperature t measured for each vent fluid sample (Seyfried et al., 2015) and at pressure $P = 80$ atm, as the

water depth was in the range 750 m to 850 m. However, PHREEQC was first used with the phreeqc.dat database to compute the limits of the stability domain of water, at $t = 90\,°C$ and $P = 80$ atm, because this database incorporates molar volumes to account for pressure influence.

As expected, it appears that pressure influence on equilibrium constants K is negligible (impact only on the 2nd or 3rd decimal in log$K$), but temperature influence is important. The stability domain of water in a (pe, pH) diagram is narrower at high temperature, with the dissociation constant of water log$Kw = -12.38$ at 90 °C, instead of -14.00 at 25 °C. The lower limit of the stability domain of water is obtained following:

$$pH + pe = -0.133 - \frac{1}{2}logf H_2, \tag{4}$$

and the upper limit as:

$$pH + pe = 16.31 + \frac{1}{4}logf O_2, \tag{5}$$

where $f H_2$ and $f O_2$ are respectively the fugacity of molecular hydrogen gas and the fugacity of molecular oxygen gas. Despite the large pressure, deviations from ideality are small, with $\phi = 0.977$ for oxygen gas and $\phi = 1.024$ for hydrogen gas in pure water, $\phi = 1$ for an ideal gas. The straight lines delimiting the stability domain of water are obtained by substituting the maximum values, *i.e.*, $f H_2 = 80$ atm and $f O_2 = 80$ atm in eqs. 4 and 5, completed with pH = 0 and pH = 12.38 (Fig. 9).

The stability domain of water spans about 12 pH units and 18 pe units at 90 °C and 80 atm *versus* 14 pH units and 21 pe units at 25 °C, 1 atm. The position of fluid samples from Lost City in this diagram will be discussed later.

4.2.3. Equilibrium calculations

Species distribution in the hydrothermal fluid was computed using PHREEQC software (Parkhurst and Appelo, 2013), with the recently reevaluated set of equilibrium constants for Fe(II) and Fe(III) species and $\Delta_f G_m^{\circ-}$ of green rusts and fougerite (Ben Nacib et al., 2016) incorporated in a modified version of the SIT database.

For sulphur, the two pKs of acidity of H_2S, present in the sit.dat database were used.

The Lost City hydrothermal fluid analyses available for sulphur
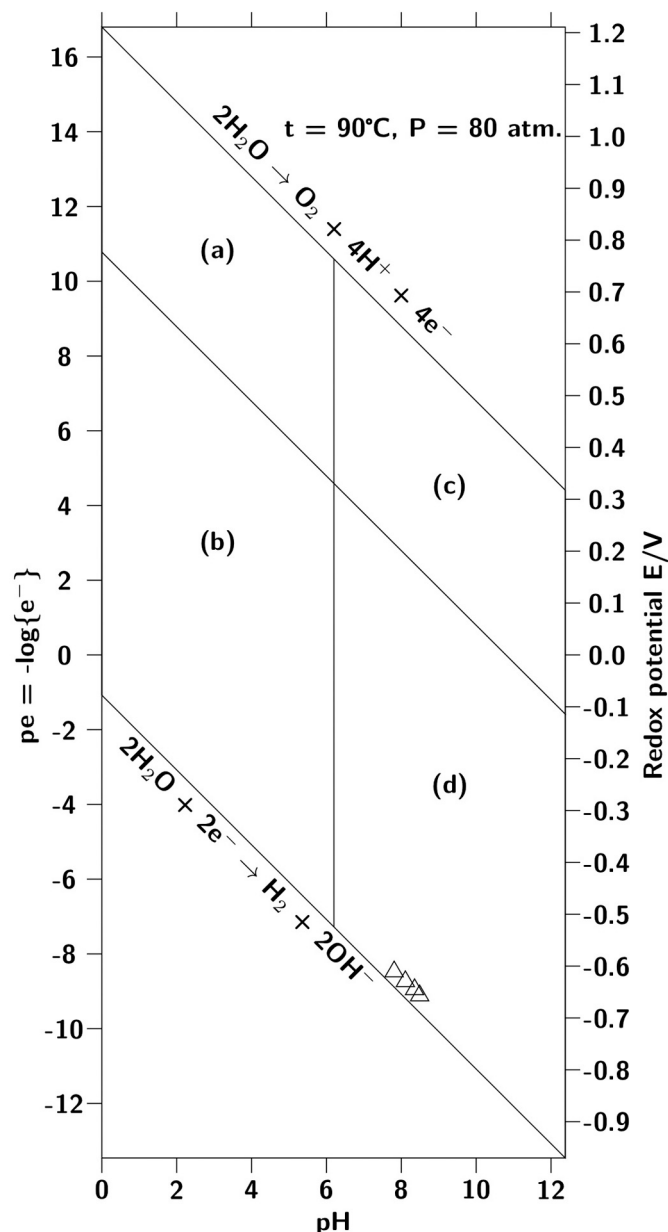
Fig. 9. Lost City hydrothermal fluids composition (open triangles) in the stability domain of water expressed as (pe, pH) at temperature $t = 90 \,°$ C, and pressure $P = 80$ atm. The corresponding ion-product constant of liquid water (Kw), defined as $Kw = \{H^+\}\{OH^-\}$, is such that $\log Kw = -12.38$; (a) oxidizing – acid; (b) reducing – acid; (c) oxidizing – alkaline; (d) reducing – alkaline conditions; upper oxidizing limit, pe + pH = 16.80; lower reducing limit, pe + pH = -1.08.

species include separately sulphate S(VI) on one hand and hydrogen sulphide (H$_2$S) on the other hand (Seyfried et al., 2015). However, sulphide was measured by titration with lead nitrate using a sulphide specific Ag/Ag$_2$S indicator electrode. Accordingly, though it is expressed as H$_2$S in Seyfried et al. (2015), it corresponds to total sulphide S(-II), including H$_2$S, HS$^-$ and S^{2-}, yielding for their concentrations:

$$[S(-II)] = [H_2S] + [HS^-] + [S^{2-}]. \tag{6}$$

Analyses performed on Lost City hydrothermal fluids are not exhaustive, in some Fe(II) concentration is missing, others lack H(0). Vent fluid data reported by Seyfried et al. (2015) include two redox couples: H(0)/H(I) and S(-II)/S(VI).

For hydrogen gas, the input for PHREEQC is [H(0)], correlated to the

analytical data by:

$$[H(0)] = 2[H_2]. \tag{7}$$

For iron, since the presence of hydrogen gas, methane and hydrogen sulphide reported at Lost City ensures that the environment is reducing, we will thus assume that any iron concentration given by Seyfried et al. (2015), here noted as Fe$_{total}$ is entirely aqueous Fe(II) as it would have been in the primordial ocean waters (Mielke et al., 2010; Branscomb and Russell, 2018b; White et al., 2020).

All other elements analyzed by Seyfried et al. (2015) were also considered in the PHREEQC calculation. It must be stressed that due to the reduced conditions, carbonate ions are absent and carbon is only present as methane C(-IV). Note that although abiotic formate and biological acetate were also detected in the Lost City fluids (Lang et al., 2010), these compounds were not considered here due to their small concentrations $36\,\mu mol\,kg^{-1}$ to $158\,\mu mol\,kg^{-1}$ for formate and $1\,\mu mol\,kg^{-1}$ to $36\,\mu mol\,kg^{-1}$ for acetate (Lang et al., 2010) and to their weak complexation affinity for iron: formate and acetate bear only one carboxylic acid which does not allow for chelatation, as opposed *e.g.*, to oxalate or citrate. Alkalinity of the solution is thus only due to OH- ion and borate as well as sulphide species.

4.3. Mineralogical control on pH: amakinite vs brucite

On the basis of the raw data as reported by Seyfried et al. (2015), namely ([Fe$_{total}$], pH on board at 25 °C), Fig. 10 shows that the Lost City fluid compositions are close to the solubility curve of Fe(OH)$_2$(cr)
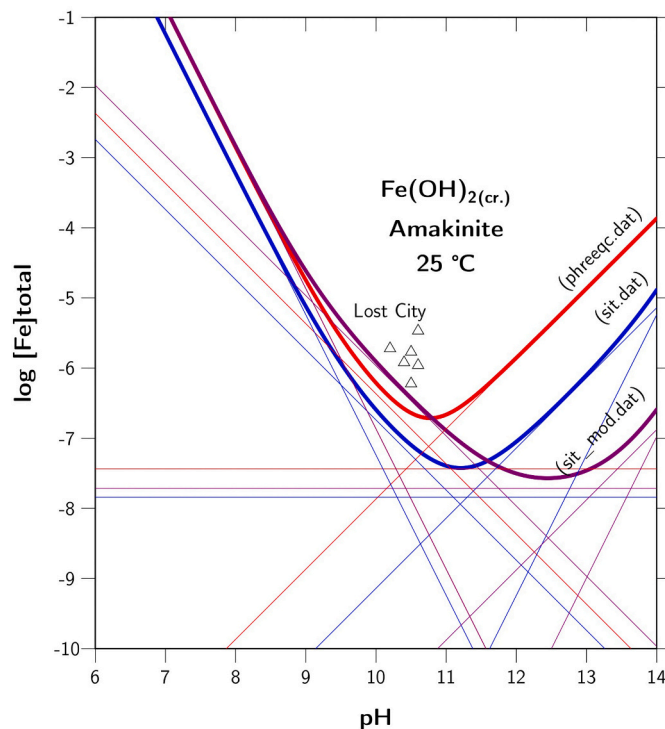
Fig. 10. Lost City hydrothermal fluid compositions (open triangles) as reported in the solubility diagram of ferrous hydroxide Fe(OH)$_2$(cr) amakinite at 25 °C, and for pH values given at 25 °C in Seyfried et al. (2015). Curves, also computed at 25 °C correspond to the three different values of solubility of amakinite at elevated pH found in the currently available databases, namely phreeqc.dat, sit.dat and modified sit.dat and new experimental data (Ben Nacib et al., 2016; Ben Nacib, 2017). The uncertainties on iron speciation at pH > 11, expressed in the three solubility curves, have no bearing; pH should be lower than 9 where temperature is higher, *e.g.*, in the root of the hydrothermal system (Seyfried et al., 2015), hence in the diagram region where all solubility curves are very close to each other.

amakinite or even oversaturated with respect to this mineral.

In the Lost City fluid samples considered here, since pH was not measured *in situ* at vent, the exact fluid pH at temperatures ranging from 75 to 116 °C (*i.e.*, the temperature of the fluids sampled at Beehive and M6 vents) is not known. While pH measured at 25 °C is about 10.5 (Seyfried et al., 2015), it should be lower at higher temperatures. The pH of a fluid at equilibrium with a serpentine (chrysotile) – tremolite - diopside assemblage would drop to 9 and 8 when temperature increases to 70 and 100 °C respectively – see Fig. 11 in Seyfried et al. (2015).

The calculations of aqueous speciation with PHREEQC were thus made considering two alternative hypotheses:

- solutions are forced to equilibrium with magnesium hydroxide Mg(OH)$_2$(cr) brucite and pH and Saturation Index (SI) of ferrous hydroxide Fe(OH)$_2$(cr) amakinite are computed;
- solutions are forced to equilibrium with Fe(OH)$_2$(cr) amakinite and pH and SI of Mg(OH)$_2$(cr) brucite are computed.

When equilibrium with Mg(OH)$_2$(cr) brucite is forced (Fig. 11, left), pH values are much lower, closer to neutrality than the values measured at 25 °C, 1 atm on board. They are in the range 8.0 to 9.2 and solutions are largely *oversaturated* with respect to Fe(OH)$_2$(cr) amakinite (Saturation indexes are positive).

Data from Table 1 in Seyfried et al. (2015). For samples on rows 1, 2 and 5, Fe analysis is lacking. Col. 1: temperature *in situ*; col. 2: pH measured at 25 °C; col. 3 and 4: pH and SI brucite computed when equilibrium is forced with amakinite; col. 5 and 6: pH and SI amakinite computed when equilibrium is forced with brucite; col. 7: difference (5)–(3).

Conversely, when equilibrium with Fe(OH)$_2$(cr) amakinite is forced, fluids are *undersaturated* with respect to brucite (Table 3), while pH values remain lower that the measured ones (Fig. 11, right).

For one Lost City sample (Beehive vent) the fluid is simultaneously in equilibrium with both brucite and amakinite. The pH differences between these two hypotheses are nonetheless small, ranging from zero to 0.6 (Table 3, column 7). Overall, pH values are much less alkaline than pH measured on board at 25 °C, on the discharged hydrothermal fluids, as predicted by Seyfried et al. (2015).

Field evidence for brucite dissolution supporting fluid undersaturation with respect to brucite (Ludwig et al., 2006) and the relatively large values reported for dissolved silica by Seyfried et al. (2015, 25 μmolkg^{-1} to 92 μmolkg^{-1}) are in favour of pH control by equilibrium with ferrous hydroxide Fe(OH)$_2$(cr) amakinite, *i.e.*, the second hypothesis. This is in agreement with field observations highlighting the occurrence of amakinite in oceanic serpentinites drilled below the Lost City alkaline hydrothermal field (Beard et al., 2009).

4.4. Equilibrium control on redox conditions

Two values for pe can be computed from the two redox couples, H(0)/H(I) and S(-II)/S(VI) established from the Lost City hydrothermal fluid analyses available in Seyfried et al. (2015) (Table 4, columns 2 and 3).

Values for pe computed from H(0)/H(I) couple range from −8.5 to −10.8 in the fluids discharged at BH vent, with even more negative values at M6 vent (−12.6). This corresponds to redox potential *Eh* values ranging from −620 mV to −645 mV. Values are not significantly modified if equilibrium with brucite is considered instead of equilibrium with amakinite: the difference is less than 10 mV. Values for pe computed from S(-II)/S(VI) couple, are less negative, about pe = −6 to −6.2, for BH, which corresponds to *Eh* from −430 mV to −455 mV, pe = −8.6 for M6 (*Eh* = −950 mV).

Brackets {} designate activities of aqueous species; col. 6: SI = log Q/K (eq. 10); col. 7: SI = log Q/K (eq. 13).

It is well known that different redox couples are separated by kinetic energy barriers and in this respect (pe, pH) diagrams can be misleading (Berner, 1971, 1981). However, as far as aqueous iron species and ferrous hydroxide are considered, it must be emphasized that corrosion studies have shown that: (i) the couple Fe^{2+}/Fe^{3+} is electroactive at the Pt electrode; (ii) that the potential measured is independent of the nature and of the area of the surface of the indicator electrode (Pt or Ag), and of stirring conditions, as verified by voltammetric studies. This overall implies that the measured potential has a true thermodynamic meaning (Refait et al., 1999). Compared to the S(-II)/S(VI) couple, which involves a series of intermediate reactions, the couple H(0)/H(I) is thus more relevant to discuss the redox conditions in relation to iron geochemistry.

4.5. Position of lost City fluids in the domain of stability of water at high temperatures and pressures

From the pe obtained and considering a pH forced at equilibrium with amakinite, data can be plotted in the stability diagram of water (Fig. 9). Lost City hydrothermal fluids are close to the lower limit of the stability domain of water, but still inside. Not surprisingly, it supports a reducing environment, in agreement with hydrogen gas emissions reported at Lost City alkaline hydrothermal vents. This strengthens the assumption that total dissolved iron is almost exclusively composed of Fe(II) species. Calculation shows that aqueous Fe(II) is distributed in several species at very close concentrations, Fe^{2+}, Fe(OH)$^+$, Fe(OH)$_2^0$,
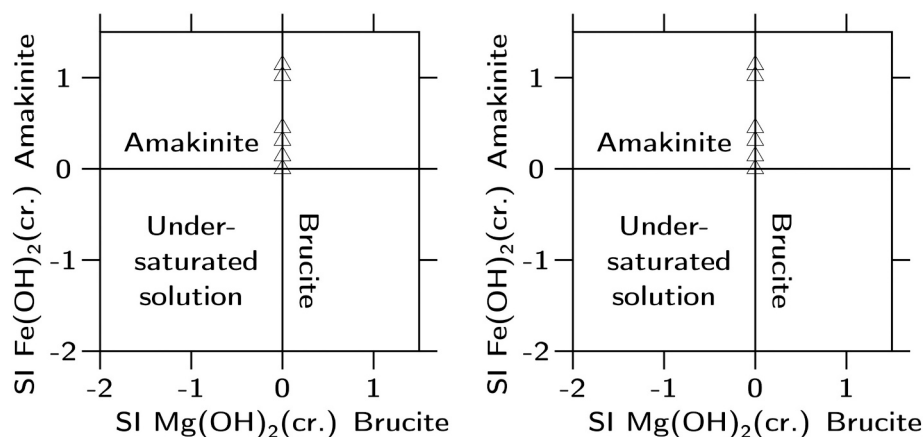

Fig. 11. Lost City hydrothermal fluid compositions (open triangles) in the equilibrium diagram Fe(OH)$_2$(cr·) amakinite - Mg(OH)$_2$(cr) brucite. The same data are plotted under two different assumptions: left: when solutions are forced to equilibrium with brucite; right: when solutions are forced to equilibrium with amakinite. SI stands for saturation index (Table 3).

Table 3

Comparison of pH under the assumption of equilibrium with brucite or with amakinite for fluids from Lost City.

Sample	t	pH at	pH eq.	SI	pH eq.	SI	ΔpH
	/°C	25 °C	Amakinite	Brucite	Brucite	Amakinite	
	1	2	3	4	5	6	7
M6-J2362IGT2	75	10.5			8.99		
M6-J2362IGT4	78	10.5			8.96		
BH-J2360IGT2	116	10.4	7.81	−0.36	7.99	0.31	0.18
BH-J2360IGT6	90	10.6	8.31	−1.72	9.16	1.14	0.85
BH-J2360CGTR	96	10.1			8.25		
BH-J2361IGT5	90	10.5	8.49	−0.18	8.58	0.14	0.09
BH-J2361IGT6	90	10.6	8.05	−1.23	8.64	1.02	0.58
BH-J2361CGTB	85	10.2	8.36	0.00	8.36	0.00	0.00
BH-J2361CGTWu	94	10.5	8.11	−0.53	8.38	0.45	0.27

Table 4

Tests of equilibria between $Fe(OH)_2$(cr) amakinite, GR1-Cl and GR2-SO4.

Sample	t	pe	pe			GR1-Cl/	GR2-SO4/
	/°C	H(0)/H(I)	S(VI)/S(-II)	log{Cl⁻}	$log\{SO_4{}^{2-}\}$	Amakinite	Amakinite
	1	2	3	4	5	6	7
M6-J2362IGT2	75	−12.61	−8.63	−0.43	−3.37	−3.65	−9.85
M6-J2362IGT4	78	−12.61	−8.7	−0.43	−3.4	−3.65	−9.86
BH-J2360IGT2	116	−8.47		−0.46	−3.39	0.46	−1.58
BH-J2360IGT6	90			−0.44	−3.41		
BH-J2360CGTR	96	−10.76		−0.45	−3.25	−1.81	−6.02
BH-J2361IGT5	90	−9.11	−6.19	−0.44	−3.35	−0.16	−2.83
BH-J2361IGT6	90			−0.44	−3.4		
BH-J2361CGTB	85	−8.95	−6.01	−0.44	−3.16	0.00	−2.31
BH-J2361CGTWu	94	−8.74		−0.44	−3.33	0.21	−2.06

Table 5

Speciation of aqueous Fe(II) species established from Lost City fluid analyses performed by Seyfried et al. (2015) on the Beehive vent structure and considering a pH forced at equilibrium with amakinite. Values in square brackets [] are log of concentrations (mol/kg); values in brackets {} are log of activities (dimensionless referred to mol/kg scale): the activity of Fe^{3+} is derived from the activity of Fe^{2+} and pe according to $\log\{Fe^{3+}\} = \log\{Fe^{2+}\} + pe - \log K$, where $\log K$ stands for the equilibrium constant of the reaction $Fe^{3+} \rightleftharpoons Fe^{2+} + e^-$, $\log K = -11.789$ at $t = 90$ °C, $P = 1$ bar.

Sample	$[Fe^{2+}]$	$[FeOH^+]$	$[FeSO_4]$	$[Fe(OH)_2]$	$[FeCl^+]$	$[FeHS^-]$	pe	$\{Fe^{2+}\}$	$\{Fe^{3+}\}$
BH-J2360IGT2	−6.94	−6.86	−7.54	−7.44	−7.51		−8.47	−6.05	−26.31
BH-J2360IGT6	−6.96	−6.71	−7.67	−7.59	−7.73				
BH-J2361IGT5	−7.35	−6.91	−8.00	−7.59	−8.12	−7.37	−9.11	−6.52	−27.42
BH-J2361IGT6	−6.40	−6.44	−7.10	−7.59	−7.17				
BH-J2361CGTB	−6.89	−6.64	−7.36	−7.62	−7.69	−6.42	−8.95	−6.06	−26.80
BH-J2361CGTWu	−6.75	−6.63	−7.36	−7.57	−7.48		−8.74	−6.75	−27.28

$FeCl^+$ and $Fe(SO_4)^0$, with some $Fe(HS)^-$ (Table 5). Aqueous Fe(II) properties are close to Mg(II) properties and do not lead to formation of colloidal species, so that total analyses of Fe can be confidently treated as consisting of total aqueous Fe. Calculation of the activity of Fe^{3+} shows extremely small values (Table 5, last column), about 21 orders of magnitude smaller than the activity of Fe^{2+}.

To summarize, Lost City hydrothermal fluids show reducing conditions (pe = − 8.82 ± 0.28), **mildly alkaline (pH = 8.19 ± 0.25), rather than strongly alkaline** when at equilibrium with $Fe(OH)_2$(cr), amakinite at $t = 90$ ° C, $P = 80$ atm. This is in favour of the occurrence of ferrous hydroxide deeper in the root of the hydrothermal system where temperature is higher and pHs are lower compared to seafloor vents where the fluids discharge. This is supported by the occurrence of amakinite reported in oceanic serpentinites drilled below the Lost City alkaline hydrothermal field (Beard et al., 2009).

## 5. Can fougerite form in oceanic alkaline hydrothermal systems?

The question now arises whether favourable conditions for the formation of fougerite may exist in oceanic alkaline hydrothermal systems,

(*i.e.*, not only at vents where hydrothermal fluid discharge but also deeper in the roots of the hydrothermal system where temperature is higher and pH lower). To this end, amakinite, previously shown to control the pH of Lost City hydrothermal fluids must partly oxidize. The stability domain of $Fe(OH)_2$(cr) is such that it can simply be oxidized by water molecules. Under anaerobic conditions, amakinite oxidized into goethite after a few months even in absence of oxygen, though it was maintained in an inert nitrogen atmosphere in a glove box (Ben Nacib, 2017). Ferrous hydroxide, amakinite, is thus thermodynamically unstable or metastable in water. It may form because the system is in steady state, with H2 emissions maintaining the system close to the lower limit of stability of water. It then can oxidize into fougerite thanks to the recurrent circulation of seawater in the hydrothermal conduits. When Fe(II) partly oxidizes in the brucitic layer, sheets separate, water enters the interlayer with anions that will equilibrate the resultant excess of positive charge appeared. This explains the large decrease in Gibbs free energy of formation observed during the transformation of ferrous hydroxide into green rusts (Fig. 6), which is mainly due to the heat consumed for the hydration of the brucitic layer (Trolard and Bourrié, 2012).

This can affect the mass balances of anions in seawater, for which

two anions are likely to enter the interlayer: chloride or sulphate. This can be discussed by computing the amakinite/GR1-Cl and amakinite/GR2-SO4 equilibria.

From the Gibbs free energies of formation of GR1-Cl and GR2-SO4, it is possible to assess equilibria between amakinite and green rust. For GR1-Cl, this gives:

$$4Fe(OH)_2(cr) + Cl^- + 2H_2O \rightleftharpoons \left[Fe(II)_3Fe(III)(OH)_8\right][Cl \cdot 2H_2O] + e^- \quad (8)$$
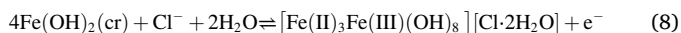
With data from Table 1 and auxiliary thermodynamic data given in Table 6, one obtains for reaction 8:

$$\Delta_r G_m^{\circ-} = -2619.250 + 4 \times 490.035 + 131.217 + 2 \times 237.140$$
$$= -53.61 \, kJ \, mol^{-1}. \quad (9)$$

This gives $logK = 9.392$ for reaction 8, and the equilibrium is checked for the aqueous solution by:

$$logQ/K = log\{Cl^-\} + pe + 2log\{H_2O(l)\} + 9.392. \quad (10)$$

From chloride analyses provided by Seyfried et al. (2015) and pe determined above from the H(0)/H(I) couple, the values of $logQ/K$ can be computed (Table 4). It must be stressed that pH is not present in eq. 10, so that the results do not depend on the validity of the assumption of pH control by equilibrium with amakinite.

The results show positive or negative values, all close to zero for Beehive vent (Table 4, column 6). Significantly, the sample BH-J2361CGTB, simultaneously at equilibrium with both amakinite and brucite, is also in equilibrium with GR1-Cl.

This means that chloride concentration in this hydrothermal system is equal to the chloride concentration value at the triple point amakinite – brucite – GR1-Cl. To explain the small concentrations of chloride observed, Seyfried et al. (2015) considered the possibility of iowaite formation. The present results suggest that chloride-fougerite, GR1-Cl, is more likely to form, as in iowaite iron is only present as Fe(III).

Similarly, for GR2-SO4, one obtains:

$$6Fe(OH)_2(cr) + SO_4^{2-} + 8H_2O \rightleftharpoons \left[Fe(II)_4Fe(III)_2(OH)12\right][SO_4 \cdot 8H_2O] + 2e^- \quad (11)$$
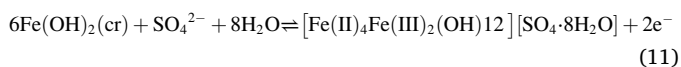
hence

$$\Delta_r G_m^{\circ-} = -5688.348 + 6 \times 490.035 + 744.004 + 8 \times 237.140$$
$$= -107.01 kJ \, mol^{-1}. \quad (12)$$

This gives $logK = 18.75$ for reaction 11, and the equilibrium is checked by:

$$logQ/K = log\{SO_4^{2-}\} + 2pe + 8log\{H_2O(l)\} + 18.75. \quad (13)$$

All values, ranging from -1.6 to -6, are negative (Table 4, column 7). This means that sulphate concentration in the reduced hydrothermal fluid is too small to promote direct formation of the GR2-SO4.

The calculations above were made at 25 °C, due to the lack of knowledge on enthalpies of reactions at higher temperatures, but errors should partly compensate as the difference between Gibbs free energies of green rusts and amakinite is considered for calculations. We can conclude that fougerite may directly form by oxidation of ferrous hydroxide into fougerite-Cl, in the Lost City hydrothermal system. As

Table 6
Auxiliary thermodynamic data at $T = 298.15K$, $P = 1$ bar from Lemire et al. (2013).

Species	$\Delta_f G_m^{\circ-}$ /kJmol^{-1}
e$^-$	0
H$_2$O(l)	−237.140
Cl$^-$	−131.217
SO$_4^{2-}$	−744.004

chloride concentration increases and H$_2$ concentration decreases, due to mixing with seawater, the formation of fougerite is favoured. Interlayers of fougerite can later accommodate other anions, such as sulphate, nitrate and lactate, as well as formate and neutral molecules such as methane. This can provide reactants for further organic syntheses of prebiotic interest in this two–dimensional reactive environment that may in addition act as a membrane. The complete absence of carbonate ions in the solutions from Lost City hydrothermal field used in this paper (related to the reducing conditions) precludes the existence of carbonate ions in the interlayer in the initial fougerite formed at the vent level. This does not preclude the occurrence of carbonate by secondary dissolution of brucite and precipitation of calcite and aragonite, that are indeed present in these environments. Carbonate ion may thus enter lately the interlayer.

Deeper in the hydrothermal system, magmatic fluids enriched in CO$_2$ can also represent a source of carbonate ions possibly integrating the interlayers of fougerite formed at higher temperature in the basement conduits and fractures where seawater circulate, deep in the crust (up to 7 km).

6. Future research targeting questions related to the emergence of life

Despite the impressive amount of experimental and thermodynamic data already available on fougerite and green rusts (section 3), the specific implications proposed for fougerite nanocrystals in questions related to life's emergence assume a number of reactions promoted by this mineral, which have not yet been experimentally tested. In the following, we enumerate some of the most relevant open questions inviting research efforts in this regard, first those that imply fougerite formation, the composition of the octahedral layer, then the interlayer anions and their reactivity:

1. Thermodynamic, structural and reaction data are needed for green rusts, including fougerite, under environmental conditions such as those reported for alkaline hydrothermal vents to constrain the stability domain of fougerite at elevated temperatures and pressures, in order to check equilibria with solutions of compositions close to the ones encountered at alkaline hydrothermal vents but also deeper in the root of the hydrothermal system. In pure MgO–FeO–H$_2$O system, and under STP conditions, amakinite and brucite precipitate separately, without forming a (Fe,Mg)(OH)$_2$ solid solution. This is probably due to differences in electronegativity between Mg(II) and Fe(II), though the electric charges are identical and their ionic radii are very close to each other (Bourrié et al., 2019). Fougerite may nonetheless form from oxidation of pure amakinite. Iron oxidation induces a net gain in positive charges in the octahedral layers, which then separate and water enters the interlayer. The process is irreversible and hydration of the layers comes with large variations of Gibbs free energy of formation (Fig. 6) and of enthalpy (Trolard and Bourrié, 2012) that need to be estimated more precisely. Moreover, it may incorporate in the octahedral layer both Mg(II) and possibly other divalent metals (Ni(II), Mn(II)) surrounding Fe(III) ions.

2. More field data are needed on the fluid composition in different alkaline hydrothermal systems. A question that arises is: did life emerge in strongly alkaline conditions or in mildly alkaline conditions, as suggested above by our results? Did the internal pH of the biota change only slightly, whereas pH of the ocean changed strongly from acidic conditions to about 8.3?

3. Does nickel in fougerite or Ni—Fe green rusts play a catalytic role such as it does in some Fe—Ni sulfides, such as Fe$_5$NiS$_8$ greigite or Fe$_2$Ni$_4$S$_8$ violarite (Russell et al., 1998)? Many experiments were performed with sulfides in hydrothermal high pressure flow reactors and in chemical gardens (Altair et al., 2021), but none with green rusts. Nickel has been shown to replace iron in the brucitic layer of fougerite. However, the reactivity of such Ni-containing green rusts

has not been assessed so far. This is of importance since in extant life the H_2-related metabolisms are most frequently carried out by Ni-Fe-catalytic centres in hydrogenase enzymes (Ménez, 2020).

4. If fougerite acts as an electron donor, by which mechanism can we regenerate Fe(II) in the brucitic layer? Are electrons supplied by electron transfer through conduction in the octahedral layer or by reactants in solution? These reactants should be different from H_2 for life to extend out of the chimneys environment. Anion exchange could play a role in this respect, with nitrate, and small organic anions. This regeneration mechanism should allow for fougerite to stay inside its stability domain, *i.e.*, in the range of Fe(III)/Fe$_{total}$ 1/4–1/3 (Fig. 5), otherwise it would transform into proto-goethite or goethite, with a crystallographic structure incompatible with membrane properties (no interlayers).

5. In the proposed scenarios for life's emergence, a precursor of ATP/ADP energy storage is required. In this respect, the condensation of phosphate to pyrophosphate or even higher polyphosphates in fougerite interlayers is envisaged (Duval et al., 2020a). However, fougerite's reactivity to phosphate is still debated while it is crucial to better understand and establish the fougerite potential for this process under specific redox conditions (*i.e.*, by considering variably reduced forms of the mineral) in so small concentrations of phosphate that fougerite would not transform into Fe(II)-Fe(III) phosphates (vivianite-strengite).

6. A crucial role for molybdenum, a two-electron transition metal, in the early stages of life is frequently inferred from both the versatility of Mo-catalysed reactions in extant life and the phylogeny of the Mo-dependent enzymes (Schoepp-Cothenet et al., 2012; Nitschke et al., 2013). The question arises then: can molybdenum, likely in the form of molybdate (MoO_4^{2-}) or thiomolybdate (MoS_4^{2-}), replace the traditionally considered interlayered anions in fougerite and more generally in green rusts? How would such an integration in between the brucitic layers affect the structural and redox properties of the Mo-bearing GR? To date, although the method is complex, no data exist beyond those provided by Itaya et al. (1987) and Rives and Ulibarri (1999) reporting the absorption of molybdate ions in a hydrotalcite-like compounds. Let us recall that hydrotalcite and fougerite are isostructural.

7. Reactivity of fougerite with simple forms of C, H and N is also a key target for future experiments and theoretical calculations. Emergence of life hypotheses that heavily rely on fougerite assume a number of reactions and structural changes that resemble crucial basic functions of microbial energy metabolism such as the binding-change and escapement mechanisms that characterize life (Branscomb et al., 2017). These reactions can be performed by fougerites representing mixtures of the cases mentioned in the above questions (1) to (4), *i.e.*, they may contain at the same time Ni and Mg cations substituting for Fe in the brucitic layers, and are "doped" with a range of different interlayered anions, including phosphates, organic ions and (thio)molybdates. Due to the presence of these compounds in alkaline hydrothermal systems and their reactivity with organic compounds, reactions to be explored are the oxidation of molecular hydrogen, the oxidation of methane, the reduction of CO_2 and CO and the production of more complex, poly- and heterocyclic organic molecules, in particular nitrogen containing molecules, *e.g.*, NAD, flavin, pterin *etc.*, possibly with the help of hydrazine $(NH_2)_2$. Hydrazine would form by dimerization from amidogen (H_2N) which is speculated as a byproduct in the oxidation of methane to methanol with NO (derived from the reduction of nitrite) as oxygen-donor (Russell and Nitschke, 2017).

A thorough experimental assessment of whether (and if yes, which of) these reactions can take place in fougerite would contribute to supporting or invalidating hypotheses related to the key role of fougerite in the alkaline hydothermal vent theory for the emergence of life and thus to experimentally advancing research on life's emergence on Earth and beyond.

References

Aguirre, V.P., Jocic, S., Webster, P., Buser, C., Moss, J.A., Barge, L.M., Tang, Y., Guo, Y., Baum, M.M., 2020. Synthesis and characterization of mixed-valent iron layered double hydroxides ("green rust"). Am. Chem. Soc. Earth Space Chem. 5, 40–54. https://doi.org/10.1021/acsearthspacechem.0c00272.

Aissa, R., Ruby, C., Géhin, A., Abdelmoula, M., Génin, J.M.R., 2004. Synthesis by coprecipitation of Al-substituted hydroxysulphate green rust Fe$^{II}_4$Fe$^{III}_2$Al$_y$(OH)$_{12}$SO$_4$·nH$_2$O. Hyperfine Interact. 156-157, 445–451.

Allada, R.K., Navrotsky, A., Berbeco, H.T., Casey, W.H., 2002. Thermochemistry and aqueous solubilities of hydrotalcite-like solids. Science 296, 721–723.

Allen, D.E., Seyfried, W.E., 2003. Alteration and mass transfer in the MgO–CaO–FeO–Fe$_2$O$_3$–SiO$_2$–Na$_2$O–H$_2$O–HCl system at 400 and 500 bars: implications for pH and compositional controls on vent fluids from ultramafic-hosted hydrothermal systems at mid-ocean ridges. Geochim. Cosmochim. Acta 67, 1531–1542.

Altair, T., Borges, L.F., Galante, D., Varela, H., 2021. Experimental approaches for testing the hypothesis of the emergence of life at submarine alkaline vents. Life 11, 777. https://doi.org/10.3390/life1108077.

Andreani, M., Ménez, B., 2019. New perspectives on abiotic organic synthesis and processing during hydrothermal alteration of the oceanic lithosphere. In: Orcutt, B., Daniel, I., Dasgupta, R. (Eds.), Deep Carbon: Past to Present. Cambridge University Press, pp. 447–479. https://doi.org/10.1017/9781108677950.

Andreani, M., Munoz, M., Marcaillou, C., Delacour, A., 2013. μXANES study of iron redox state in serpentine during oceanic serpentinization. Lithos 178, 70–83.

Anthony, J.W., Bideaux, R.A., Bladh, K.W., Nichols, M.C., 1997. Halides, hydroxides, oxides, volume 3. Mineralogical Society of America.

Arndt, N., 2011. White smoker. In: Gargaud, M., Amils, R., Cernicharo Quintanilla, J., Cleaves, H.J., Irvine, W.M., Pinti, D.L., Viso, M. (Eds.), Encyclopedia of Astrobiology. Springer, p. 1779. https://doi.org/10.1007/978-3-642-11274-4_1691.

Avery, B.W., 1973. Soil classification in the Soil survey of England and Wales. J. Soil Sci. 24, 324–338.

Ayala-Luis, K.B., Koch, C.B., Hansen, H.C.B., 2010. One-pot synthesis and characterization of FeII-FeIII hydroxide (green rust) intercalated with C9-C14 linear alkyl carboxylates. Appl. Clay Sci. 50, 512–519.

Baize, D., Girard, M.C. (Eds.), 2009. Référentiel pédologique 2008. AFES, Éditions Quae.

Barge, L., Flores, E., Baum, M.B., VanderVelde, D.G., Russell, M.J., 2019. Redox and pH gradients drive amino acid synthesis in iron oxyhydroxide mineral systems. Proc. Natl. Acad. Sci. 116, 4828–4833. https://doi.org/10.1073/pnas.1812098116.

Bearcock, J., Perkins, W., Dinelli, E., 2006. Fe(II)/Fe(III) "green rust" developed within ochreous coal mine drainage sediment in South Wales, UK. Mineral. Mag. 70, 731–741.

Beard, J.S., Frost, B.R., Fryer, P., McCaig, A., Searle, R., Ildefonse, B., Zinin, P., Sharma, S.K., 2009. Onset and progression of serpentinization and magnetite formation in olivine-rich troctolite from IODP Hole U1309D. J. Petrol. 50, 387–403. https://doi.org/10.1093/petrology/egp004.

Ben Nacib, J., 2017. Rôle des oxydes de fer dans la mobilité de métaux et de métalloïdes et application aux interactions sols-solutions. Thèse de doctorat. Université d'Avignon et des Pays de Vaucluse et Institut National Agronomique de Tunis.

Ben Nacib, J., Bourrié, G., Ben Thayer, B., Trolard, F., 2016. A consistent set of thermodynamic data for iron and reevaluation of Green Rusts and fougerite solubilities. J. Environ. Sci. Eng. 5, 383–396. https://doi.org/10.17265/2162-5298/2016.08.001.

Bernal, J.D., Dasgupta, D.T., Mackay, A.L., 1959. The oxides and hydroxides of iron and their structural interrelationships. Clay Min. Bull. 4, 15–30.

Berner, R.A., 1971. Principles of Chemical Sedimentology. McGraw Hill.

Berner, R.A., 1981. Kinetics of weathering and diagenesis. In: Lasaga, A., Kirkpatrick, R. (Eds.), Kinetics of Geochemical Processes, Mineralogical Society of America. volume 8 of Reviews in Mineralogy, pp. 111–134.

Bhave, C., Shejwalkar, S., 2017. A review on the synthesis and applications of green rust for environmental pollutant remediation. Int. J. Environ. Sci. Technol. 25, 1243–1248.

Bocher, F., Géhin, A., Ruby, C., Ghanbaja, J., Abdelmoula, M., Génin, J.M.R., 2004. Coprecipitation of Fe(II–III) hydroxycarbonate green rust stabilised by phosphate adsorption. Solid State Sci. 6, 117–124.

Bond, D., Fendorf, S., 2003. Kinetics and structural constraints of chromate reduction by green rusts. Environ. Sci. Technol. 37, 2750–2757.

Boschi, C., Dini, A., Baneschi, F., Perchiazzi, N., Cavallo, A., 2017. Brucite-driven CO_2 uptake in serpentinized dunites (Ligurian Ophiolites, Montecastelli, Tuscany). Lithos 288-289, 264–281.

Bourrié, G., Trolard, F., Refait, P., Feder, F., 2004. A solid solution model for Fe(II)-Fe (III)-Mg(II) green rusts and fougerite and estimation of their Gibbs free energies of formation. Clay Clay Miner. 52, 382–394.

Bourrié, G., Ben Nacib, J., Ona-Nguema, G., Trolard, F., 2019. Absence of solid solution between Fe(II) and Mg(II) hydroxides and consequences on formation of fougerite and smectites. In: Chudaev, O., Kharaka, Y., Harmon, R., Millot, R., Shoukar-Stash, O. (Eds.), 16th International Symposium on Water-Rock Interaction (WRI-16) and 13th International Symposium on Applied Isotope Geochemistry (1st IAGC International Conference), EDP Sciences, vol. 98, pp. 1–5. https://doi.org/10.1051/e3sconf/20199804003.

Branscomb, E., Russell, M.J., 2018a. Frankenstein or a submarine alkaline vent: who is responsible for abiogenesis? Part 1: what is life – that it might create itself? Bioessays 40, 1700179.

Branscomb, E., Russell, M.J., 2018b. Frankenstein or a submarine alkaline vent: who is responsible for abiogenesis? Part 2: as life is now, so it must have been in the beginning. Bioessays 40, 1700182.

Branscomb, E., Biancalani, T., Goldenfeld, N., Russell, M.J., 2017. Escapement mechanisms and the conversion of disequilibria; the engines of creation. Phys. Rep. 377, 1–60.

Chaudhuri, S., Lack, Joseph G., Coates, John D., 2001. Biogenic magnetite formation through anaerobic biooxidation of Fe(II). Appl. Environ. Microbiol. 67, 2844–2848.

Choi, J., Batchelor, B., 2008. Nitrate reduction by fluoride green rust modified with copper. Chemosphere 70, 1108–1116.

Christiansen, B., Balic-Zunic, T., Petit, P., Frandsen, C., Mörup, S., Geickeis, H., Katerionopoulou, A., Stipp, S., 2009. Composition and structure of an iron-bearing, layered double hydroxide (LDH): greeen rust sodium sulphate. Geochim. Cosmochim. Acta 73, 3579–3592.

Christiansen, B., Dideriksen, K., Katz, A., Nedel, S., Bovet, N., Sørensen, H., Frandsen, C., Gundlach, C., Andersson, M., Stipp, S., 2014. Incorporation of monovalent cations in sulfate green rust. Inorg. Chem. J. 53, 5557–5894.

Cornell, R.M., Schwertmann, U., 2003. The Iron Oxides. VCH.

Drissi, S., Refait, P., Génin, J.M.R., 1994. The oxidation of Fe(OH)₂ in the presence of carbonate ions: structure of carbonate green rust one. Hyperfine Interact. 90, 395–400.

Drissi, S., Refait, P., Abdelmoula, M., Génin, J.M., 1995. The preparation and thermodynamic properties of Fe(II)–Fe(III) hydroxide–carbonate (green rust one) — Pourbaix diagram of iron in carbonate–containing aqueous media. Corros. Sci. 37, 2025–2041.

Duval, S., Branscomb, E., Trolard, F., Bourrié, G., Grauby, O., Heresanu, V., Schoepp-Cothenet, B., Zuchan, K., Russell, M.J., Nitschke, W., 2020a. On the why's and how's of clay minerals' importance in life's emergence. Appl. Clay Sci. 195, 1–7. URL.

Duval, S., Zuchan, K., Baymann, F., Schoepp-Cothenet, B., Branscomb, E., Russell, M.J., Nitschke, W., 2020b. Minerals and the emergence of life. In: Kroneck, P., Sosa-Torres, M. (Eds.), Metals in Life Sciences, volume 21. Walter de Gruyter, pp. 135–157 chapter 5.

Erbs, M., Hansen, H., Olsen, C., 1999. Reductive dechlorination of carbon tetrachloride using Iron(II) Iron (III) hydroxide sulfate (green rust). Environ. Sci. Technol. 33, 307–311.

Etique, M., Zegeye, A., Grégoire, B., Carteret, C., Ruby, C., 2014. Nitrate reduction by mixed iron (II-III) hydroxycarbonate green rust in the presence of phosphate anions: the key parameters influencing the ammonium selectivity. Water Res. 62, 29–39.

Etique, M., Jorand, F.P., Ruby, C., 2016. Magnetite as aprecursor for green rust through the hydrogenotrophic activity of the iron-reducing bacteria *Shewanella putrefaciens*. Geobiology 14, 237–254. https://doi.org/10.1111/gbi.12170.

Feder, F., Trolard, F., Klingelhöfer, G., Bourrié, G., 2005. *In situ* Mössbauer spectroscopy — evidence for green rust (Fougerite) in a gleysol and its mineralogical transformations with time and depth. Geochim. Cosmochim. Acta 69, 4463–4483.

Feder, F., Trolard, F., Bourrié, G., Klingelhöfer, G., 2018. Quantitative estimation of fougerite green rust in soils and sediments by citrate – bicarbonate kinetic extractions. Soil Syst. 2 https://doi.org/10.3390/soilsystems2040054. URL: http://www.mdpi.com/journal/soilsystems.

Fleischer, M., 1962. New mineral names. Am. Mineral. 47, 1216–1223.

Fonseca, I., Feio, M., Lino, A., Reis, M., Rainha, V., 1998. The influence of the media on the corrosion of mild steel by *Desulfovibrio desulfuricans* bacteria: an electrochemical study. Electrochim. Acta 43, 213–222.

Fouquet, Y., 2011. Black smoker. In: Gargaud, M., Amils, R., Cernicharo Quintanilla, J., Cleaves, H.J., Irvine, W.M., Pinti, D.L., Viso, M. (Eds.), Encyclopedia of Astrobiology. Springer, p. 213. https://doi.org/10.1007/978-3-642-11274-4_201.

Foustoukos, D.I., Savov, I.P., Janecky, D.R., 2008. Chemical and isotopic constraints on water/rock interactions at the Lost City hydrothermal field, 30N Mid-Atlantic Ridge. Geochim. Cosmochim. Acta 72, 5457–5474.

Fredrickson, J., Zachara, J., Kennedy, D., Dong, H., Onstott, T., Hinman, N., Li, S., 1998. Biogenic iron mineralization accompanying the dissimilatory reduction of hydrous ferric oxide by a groundwater bacterium. Geochim. Cosmochim. Acta 62, 3239–3257.

Früh-Green, G.L., Kelley, D.S., Bernasconi, S.M., Karson, J.A., Ludwig, K.A., Butterfield, D.A., Boschi, C., Proskurowski, G., 2003. 30,000 years of hydrothermal activity at the Lost City vent field. Science 301, 495–498. https://doi.org/10.1126/science.1085582.

Géhin, A., Ruby, C., Abdelmoula, M., Benali, O., Ghanbaja, J., Refait, P., Génin, J.M.R., 2002. Synthesis of Fe(II, III) hydroxysulphate green rust by coprecipitation. Solid State Sci. 4, 61–66.

Génin, J.M., Olowe, A., Refait, P., Simon, L., 1996. On the stoichiometry and Pourbaix diagram of Fe(II)-Fe(III) hydroxy-sulphate or sulphate-containing green rust 2: an electrochemical and Mössbauer spectroscopy study. Corros. Sci. 38, 1751–1762.

Génin, J.M.R., Bourrié, G., Trolard, F., Abdelmoula, M., Jaffrezic, A., Refait, P., Maitre, V., Humbert, B., Herbillon, A., 1998. Thermodynamic equilibria in aqueous suspensions of synthetic and natural FeII–FeIII green rusts : occurrences of the mineral in hydromorphic soils. Environ. Sci. Technol. 32, 1058–1068.

Génin, J.M.R., Aïssa, R., Géhin, A., Abdelmoula, M., Benali, O., Ernstsen, V., Ona-Nguema, G., Upadhyay, C., Ruby, C., 2005. Fougerite and FeII–III hydroxycarbonate green rust; ordering, deprotonation and/or cation substitution; structure of hydrotalcite-like compounds and mythic ferrosic hydroxide Fe(OH)₂₊ₓ. Solid State Sci. 7, 545–572.

Georgieva, M.N., Little, C.T., Maslennikov, V.V., Glover, A.G., Ayupova, N.R., Herrington, R.J., 2021. The history of life at hydrothermal vents. Earth Sci. Rev. 103602. URL: https://www.sciencedirect.com/science/article/pii/S0012825221001021. https://doi.org/10.1016/j.earscirev.2021.103602.

Girard, A., Chaudron, G., 1935. Sur la constitution de la rouille. Comptes Rendus de l'Académie des Sciences, Paris 200, 127–129.

Glasauer, S., Langley, S., Beveridge, T., 2002. Intracellular iron minerals in a dissimilatory iron-reducing bacterium. Science 295, 117–119.

Guerbois, D., Ona-Nguema, G., Guillaume, M., Moustapha, A., Laverman, A., Mouchel, J., Barthelemy, K., Maillot, F., Brest, J., 2014. Nitrite reduction by biogenic hydroxycarbonate green rusts: evidence for hydroxy-nitrite green rust formation as an intermediate reaction product. Environ. Sci. Technol. 48, 4505–4514.

Guilbaud, R., White, M.L., Poulton, S.W., 2013. Surface charge and growth of sulphate and carbonate green rust in aqueous media. Geochim. Cosmochim. Acta 108, 141–153. URL: http://www.sciencedirect.com/science/article/pii/S0016703713000392. https://doi.org/10.1016/j.gca.2013.01.017.

Halevy, I., Bachan, A., 2017. The geologic history of seawater pH. Science 355, 1069–1071.

Halevy, I., Alesker, M., Schuster, E.M., Popovitz-Biro, R., Feldman, Y., 2017. A key role for green rust in the Precambrian oceans and the genesis of iron formations. Nat. Geosci. https://doi.org/10.1038/NGEO2878.

Hansen, H.C.B., Koch, C.B., 1998. Reduction of nitrate to ammonium by sulphate green rust: activation energy and reaction mechanism. Clay Miner. 33, 87–101.

Hansen, H.C.B., Poulsen, I., 1999. Interaction of synthetic sulphate "green rust" with phosphate and the crystallization of vivianite. Clay Clay Miner. 47, 312–318.

Hansen, H.C.B., Borggaard, O., Sørensen, J., 1994a. Evaluation of the free energy of formation of Fe(II)-Fe(III) hydroxide-sulphate (green rust) and its reduction of nitrite. Geochim. Cosmochim. Acta 58, 2599–2608.

Hansen, H.C.B., Koch, C.B., Taylor, R., 1994b. Synthesis and characterization of cobalt (II)-iron(III) hydroxycarbonate, a layered double hydroxide belonging to the pyroaurite group. J. Solid State Chem. 113, 46–53.

Hansen, H.C.B., Koch, C.B., Nancke-Krogh, H., Borggaard, O.B., Sørensen, J., 1996. Abiotic nitrate reduction to ammonium : key role of green rust. Environ. Sci. Technol. 30, 2053–2056.

Hudson, R., de Graaf, R., Strandoo Rodin, M., Ohno, A., Lane, N., McGlynn, S.E., Yamada, Y.M.A., Nakamura, R., Barge, L.M., Braun, D., Sojo, V., 2020. CO_2 reduction driven by a pH gradient. Proc. Natl. Acad. Sci. 117, 22873–22879. URL: https://www.pnas.org/content/117/37/22873. https://doi.org/10.1073/pnas.2002659117. arXiv:https://www.pnas.org/content/117/37/22873.full.pdf.

Itaya, K., Chang, H.C., Uchida, I., 1987. Anion-exchanged clay (hydrotalcite-like compounds) modified electrodes. Inorg. Chem. 26, 621–626. https://doi.org/10.1021/ic00251a028.

IUSS Working Group WRB, 2014. World reference base for soil resources. In: Number 106 in World Soil Resources Reports. FAO, Roma.

Johnson, T., Bullen, T., 2003. Selenium isotope fractionation during reduction by Fe(II)-Fe(III) hydroxide-sulphate (green rust). Geochim. Cosmochim. Acta 67, 413–419.

Johnson, C.A., Freyer, G., Fabisch, M., Caraballo, M.A., Küsel, K., Hochella, M.F., 2014. Observation and assessment of iron oxide and green rust nanoparticles in metal-polluted mine drainage within a steep redox gradient. Environ. Chem. 11, 377–391.

Jolivet, J.P., 2000. Metal Oxide Chemistry and Synthesis. Wiley.

Jolivet, J.P., Henry, M., Livage, J., 1994. De la solution à l'oxyde. Savoirs actuels, InterÉditions/CNRS Éditions.

Kelley, D., Karson, J., Blackman, D., Früh-Green, G., Butterfield, D., Lilley, M., Olson, E., Schrenk, M., Roe, K., Lebon, G., Rivizzigno, P., AT3-60 shipboard party, 2001. An off-axis hydrothermal vent field near the Mid-Atlantic Ridge at 30 N. Nature 412, 145–149.

Kelley, D., Karson, J., Früh-Green, G., Yoerger, D., Shank, T., Butterfield, D., Hayes, J., Schrenk, M., Olson, E., Proskurowski, G., Jakuba, M., Bradley, A., Larson, B., Ludwig, K., Glickson, D., Buckman, K., Bradley, A., Brazelton, W., Roe, K., Elend, M., Delacour, A., Bernasconi, S., Lilley, M., Baross, J., Summons, R., Sylva, S., 2005. A serpentinite-hosted ecosystem: the Lost City hydrothermal field. Science 307, 1428–1434.

Klein, F., Bach, W., Jöns, N., McCollom, T., Moskowitz, B., Berquó, T., 2009. Iron partitioning and hydrogen generation during serpentinization of abyssal peridotites from 15°N on the Mid-Atlantic Ridge. Geochim. Cosmochim. Acta 73, 6868–6893.

Konn, C., Charlou, J.L., Donval, J.P., Holm, N.G., Dehairs, F., Bouillon, S., 2009. Hydrocarbons and oxidized organic compound in hydrothermal fluids from Rainbow and lost City ultramafic-hosted vents. Chem. Geol. 258, 299–314.

Kozlov, I.T., Levshov, P.P., 1962. Amakinite, a new mineral of the brucite-pyrochroite group. Zapiskii Vserossiyskogo Mineralogischeskogo Obshchestva 91, 72–77.

Kukkadapu, R.S., Zachara, J.M., Fredrickson, J.K., Kennedy, D.W., 2006. Biotransformation of two-line silica ferrihydrite by a dissimilatory Fe(III) reducing bacterium: formation of carbonate green-rust in the presence of phosphate. Geochim. Cosmochim. Acta 68, 2799–2814.

Lang, S.Q., Butterfield, D.A., Schulte, M., Kelley, D.S., Lilley, M.D., 2010. Elevated concentrations of formate, acetate and dissolved organic carbon found at the lost City hydrothermal field. Geochim. Cosmochim. Acta 74, 941–952, 10.1016. gca.2009.10.045.

Lang, S.Q., Früh-Green, G.L., Bernasconi, S.M., Lilley, M.D., Proskurowski, G., Mehay, S., 2012. Microbial utilization of abiogenic carbon and hydrogen in a serpentinite-hosted system. Geochim. Cosmochim. Acta 92, 82–99.

Larese-Casanova, P., Scherer, M., 2008. Abiotic transformation of hexahydro-1,3,5-trinitro-1,3,5-triazine (RDX) by green rust. Environ. Sci. Technol. 42, 3975–3981.

Latta, D., Boyanov, M., Kemner, K., O'Loughlin, E., Scherer, M., 2015. Reaction of uranium (VI) with green rusts: effect of interlayer anion. Curr. Inorg. Chem. 5, 156–168.

Lee, W., Batchelor, B., 2002. Abiotic reductive dechlorination of chlorinated ethylenes by iron bearing soils minerals. 2. Green rust. Environ. Sci. Technol. 36, 5348–5354.

Legrand, L., Abdelmoula, M., Géhin, A., Chaussé, A., Génin, J.M.R., 2001. Electrochemical formation of a new Fe(II)-Fe(III) hydroxycarbonate green rust: characterisation and morphology. Electrochim. Acta 46, 1815–1822.

Lemire, R.J., Berner, U., Musikas, C., Palmer, D.P., Taylor, P., Tochiyama, O., 2013. Chemical thermodynamics of iron-Part 1. In: volume 13a of *Chemical Thermodynamics*. OECD Nuclear Agency, Data Bank.

Lewis, J., 1997. Factors influencing the stability and properties of green rusts. In: Auerswald, K., Stanjek, H., Bigham, J. (Eds.), Soils and Environment. Catena Verlag, pp. 345–372 volume 30 of Advances in GeoEcology.

Loyaux-Lawniczak, S., Refait, P., Ehrhardt, J.J., Lecomte, P., Génin, J.M.R., 1999. The reduction of chromate ions by Fe(II) layered hydroxides. Hydrol. Earth Syst. Sci. 3, 593–599.

Loyaux-Lawniczak, S., Refait, P., Ehrhardt, J.J., Lecomte, P., Génin, J.M.R., 2000. Trapping of Cr by formation of ferrihydrite during the reduction of chromate ions by Fe(II) — Fe(III) hydroxysalt green rusts. Environ. Sci. Technol. 34, 438–443.

Ludwig, K.A., Kelley, D.S., Butterfield, D.A., Nelson, B.K., Früh-Green, G., 2006. Formation and evolution of carbonate chimneys at the Lost City Hydrothermal Field. Geochim. Cosmochim. Acta 70, 3625–3645. URL. http://www.sciencedirect.com/science/article/pii/S0016703706001840. https://doi.org/10.1016/j.gca.2006.04.016.

Maithreepala, R., Doong, R., 2005. Enhanced dechlorination of chlorinated methanes and ethenes by chloride green rusts in the presence of copper(II). Environ. Sci. Technol. 39, 4082–4090.

Marteinsson, V.T., Kristj'ansson, J.K., Kristmanssd'ottir, H., Dahlkvist, M., Sæmundsson, K., Hannington, M., Pétursd'ottir, S.K., Geptner, A., Stoffers, P., 2001. Discovery of giant submarine smectite cones on the seafloor in Eyjafjordur, Northern Iceland, and a novel thermal microbial habitat. Appl. Environ. Microbiol. 67, 827–833.

McGill, I., McEnaney, B., Smith, D., 1976. Crystal structure of green rust formed by corrosion of cast iron. Nature 29, 200–201.

McLeod, G., McKeown, C., Hall, A., Russell, M.J., 1994. Hydrothermal and oceanic pH conditions of possible relevance to the origin of life. Orig. Life Evol. Biosph. 24, 19–41.

Ménez, B., 2020. Abiotic hydrogen and methane: fuels for life. Elements 16, 39–46. https://doi.org/10.2138/gselements.16.1.39.

Ménez, B., Pisapia, C., Andreani, M., Jamme, F., Vanbellingen, Q.P., Brunelle, A., Richard, L., Dumas, P., Réfrégiers, M., 2018. Abiotic synthesis of amino acids in the recesses of the oceanic lithosphere. Nature 564, 59–63.

Mielke, R., Russell, M., Wilson, P., McGlynn, S., Coleman, M., Kidd, R., Kanik, I., 2010. Design, fabrication, and test of a hydrothermal reactor for origin-of-life experiments. Astrobiology 10, 799–810. https://doi.org/10.1089/ast.2009.0456.

Misawa, T., 1973. The thermodynamic consideration for Fe-H2O system at 25. Corros. Sci. 13, 659–676.

Murad, E., 1990. Application of [57]Fe Mössbauer spectroscopy to problems in clay minerals and soil science: possibilities and limitations. Adv. Soil Sci. 12, 125–157.

Myneni, S., Tokunaga, T., Brown, G., 1997. Abiotic selenium redox transformations in the presence of Fe(II,III) oxides. Science 278, 1106–1109.

Nagies, F., Heusler, K.E., 1998. Corrosion of metallic materials in hot salt brines. Electrochim. Acta 43, 41–51.

Nakamura, T., Nakamuta, Y., 1996. X-ray study of PCP from the Murchison CM carbonaceous chondrite. In: Proceedings of the National Institute of Polar Research Symposium on Antarctic Meteorites, National Institute of Polar Research, pp. 37–50.

Nitschke, W., Russell, M.J., 2012. Redox bifurcations: mechanisms and importance to life now, and at its origin: a widespread means of energy conversion in biology unfolds…. Bioessays 34, 106–109.

Nitschke, W., McGlynn, S.E., Milner-White, E.J., Russell, M.J., 2013. On the antiquity of metalloenzymes and their substrates in bioenergetics. Biochimica et Biophysica Acta (BBA) – Bioenergetics 1827, 871–881. URL. http://www.sciencedirect.com/science/article/pii/S0005272813000340. https://doi.org/10.1016/j.bbabio.2013.02.008.

O'Loughlin, E.J., Burris, D., 2004. Reduction of halogenated ethane by green rust. Environ. Toxicol. Chem. 23, 41–48.

O'Loughlin, E.J., Kelly, S., Cook, R., Csencsits, R., 2003a. Reduction of Uranium (VI) by mixed iron(II) /iron(III) hydroxide (green rust): formation of UO2 nanoparticles. Environ. Sci. Technol. 44, 4570–4576.

O'Loughlin, E.J., Kelly, S.D., Kemner, K.M., Csencsits, R., Cook, R.E., 2003b. Reduction of Ag^{I}, Au^{III}, Cu^{II} and Hg^{II} by Fe^{II}/Fe^{III} hydroxysulfate green rust. Chemosphere 53, 437–446.

O'Loughlin, E.J., Gorski, C., Scherer, M., Boyanov, M., Kemner, K., 2010. Effects of oxyanions, natural organic matter and bacterial cell numbers on the bioreduction of lepidocrocite (γ-FeOOH) and the formation of secondary mineralization products. Environ. Sci. Technol. 44, 4570–4576.

Ona-Nguema, G., Abdelmoula, M., Jorand, F., Benali, O., Géhin, A., Block, J.C., Robert, G.J.M., 2002. Iron(II,III) hydroxycarbonate green rust formation and stabilization from lepidocrocite bioreduction. Environ. Sci. Technol. 36, 16–20. https://doi.org/10.1021/es0020456.

Pankte, C., Obst, M., Benzerara, K., Morin, G., Ona-Nguema, G., Dippon, U., Kappler, A., 2011. Green rust formation during Fe(II) oxidation by the nitrate-reducing *Acidovorax Sp.* Strain BoFeN1. Environ. Sci. Technol. 46, 1439–1446.

Parkhurst, D., Appelo, C., 2013. Description of input and examples for PHREEQC (Version 3) — a computer program for speciation, batch-reaction, one-dimensional transport, and inverse geochemical calculations. In: Technical Report 6. U.S. Department of the Interior, U.S. Geological Survey. URL. http://pubs.usgs.gov./tm/06/a43.

Parmar, N., Gorby, Y., Beveridge, T., Ferris, F., 2001. Formation of green rust and immobilization of nickel in response to bacterial reduction of hydrous ferric oxide. Geomicrobiol J. 18, 375–385. https://doi.org/10.1080/014904501753210549.

Perez, J., Mangayayam, M., Navaz Rubio, S., Freeman, H., Tobler, D., Benning, L., 2018. Intercalation of aromatic sulfonates in green rust via ion exchange. Energy Procedia 146, 179–187.

Peulon, S., Legrand, L., Antony, H., Chausse, A., 2003. Electrochemical deposition of thin films of green rusts 1 and 2 on inert gold substrate. Electrochem. Commun. 5, 208–213.

Peulon, S., Baraize, Q., Chausse, A., 2007. Iron compounds electrodeposited onto a transparent semiconductor: synthesis and characterization by UV-vis spectroscopy. Electrochim. Acta 52, 7681–7688.

Pignatelli, I., Marrocchi, Y., Vacher, L.G., Delon, R., Gounelle, M., 2016. Multiple precursors of secondary mineralogical assemblages in CM chondrites. Meteorit. Planet. Sci. 51, 785–805. https://doi.org/10.1111/maps.12625.

Proskurowski, G., Lilley, M.D., Kelley, D.S., Olson, E., 2008a. Low temperature volatile production at the Lost City hydrothermal field, evidence from a hydrogen stable isotope geothermometer. Chem. Geol. 229, 331–343.

Proskurowski, G., Lilley, M.D., Seewald, J., Fruh-Green, G., Olson, E., Lupton, J., Sylva, S., Kelley, D.S., 2008b. Abiogenic hydrocarbon production at Lost City hydrothermal field. Science 319, 604–607.

Refait, P., Génin, J.M.R., 1993. The oxidation of ferrous hydroxide in chloride-containing aqueous media and Pourbaix diagrams of green rust one. Corros. Sci. 34, 797–819.

Refait, P., Abdelmoula, M., Génin, J.M.R., 1998a. Mechanisms of formation and structure of green rust one in aqueous corrosion of iron in the presence of chloride ions. Corros. Sci. 40, 1547–1560.

Refait, P., Charton, A., Génin, J.M.R., 1998b. Identification, composition, thermodynamic and structural properties of a pyroaurite-like iron(II)-iron(III) hydroxy-oxalate Green Rust. Eur. J. Solid State Inorg. Chem. 35, 655–666.

Refait, P., Bon, C., Simon, L., Bourrié, G., Trolard, F., Bessière, J., Génin, J.M.R., 1999. Chemical composition and Gibbs standard free energy of formation of Fe(II)-Fe(III) hydroxysulphate green rust and Fe(II) hydroxide. Clay Miner. 34, 499–510.

Refait, P., Simon, L., Génin, J.M.R., 2000. Reduction of SeO$_4$$^{2-}$ anions and anoxic formation of Fe(II) - Fe(III) hydroxy-selenate green rust. Environ. Sci. Technol. 34, 819–825.

Refait, P., Abdelmoula, M., Trolard, F., Génin, J.M.R., Ehrhardt, J.J., Bourrié, G., 2001. Mössbauer and XAS study of a green rust mineral; the partial substitution of Fe^{2+} by Mg^{2+}. Am. Mineral. 86, 731–739.

Rennert, T., Eusterhues, K., De Andrade, V., Totsche, K.U., 2012. Iron species in soils on a mofette site studied by Fe K-edge X-ray absorption near-edge spectroscopy. Chem. Geol. 332-333, 116–123.

Rives, V., Ulibarri, M., 1999. Layered double hydroxides (LDH) intercalated with metal coordination compounds and oxometalates. Coord. Chem. Rev. 181, 61–120.

Roh, Y., Lee, S., Elless, M., Foss, J., 2000. Incorporation of radioactive contaminants into pyroaurite-like phase by electrochemical synthesis. Clay Clay Miner. 48, 266–271.

Ruby, C., Géhin, A., Abdelmoula, M., Génin, J.M.R., Jolivet, J.P., 2003. Coprecipitation of Fe(II) and Fe(III) cations in sulphated aqueous medium and formation of hydroxy sulphated green rust. Solid State Sci. 5, 1055–1062.

Ruby, C., Géhin, A., Aissa, R., Ghanbaja, J., Abdelmoula, M., Génin, J.M.R., 2006. Chemical stability of hydroxysulphate green rust synthesized in the presence of foreign anions: carbonate, phosphate and silicate. Hyperfine Interact. 167, 803–807.

Russell, M., 2018. Green rust: the simple organizing "seed" of all life? Life 8, 35. https://doi.org/10.3390/life8030035.

Russell, M., Arndt, N.T., 2005. Geodynamic and metabolic cycles in the Hadean. Biogeosciences 2, 97–111.

Russell, M., Nitschke, W., 2017. Methane: fuel or exhaust at the emergence of life? Astrobiology 17, 1053–1066.

Russell, M.J., Hall, A.J., Turner, D., 1989. In vitro growth of iron sulphide chimneys: possible culture chambers for origin-of-life experiments. Terra Nova 1, 238–241.

Russell, M.J., Daia, D.E., Hall, A.J., 1998. The emergence of life from FeS bubbles at alkaline hot springs in an acid ocean. In: Wiegel, J., Adams, M.W.W. (Eds.), Thermophiles: The Keys to Molecular Evolution and the Origin of Life. Taylor and Francis, pp. 77–126.

Sabot, R., Jeannin, M., Gadouleau, M., Guo, Q., Sicre, E., Refait, P., 2007. Influence of lactate ions on the formation of rust. Corros. Sci. 49, 1610–1624.

Schellenger, A., Larese-Casanova, P., 2013. Oxygen isotope indicators of selenite reaction with Fe(II) and Fe(III) hydroxides. Environ. Sci. Technol. 47, 6254–6262.

Schlüter, K., 2000. Review: evaporation of mercury from soils – an integration and synthesis of current knowledges. Environ. Geol. 39, 249–271.

Schoepp-Cothenet, B., van Lis, R., Philippot, P., Magalon, A., Russell, M.J., Nitschke, W., 2012. The ineluctable requirement for the trans-iron elements molybdenum and/or tungsten in the origin of life. Sci. Rep. 2, 263.

Schwarzenbach, E.M., Steele-MacInnis, M., 2020. Fluids in submarine mid-ocean ridge hydrothermal settings. Elements 16, 389–394.

Schwertmann, U., Fechter, H., 1994. The formation of green rust and its transformation to lepidocrocite. Clay Miner. 29, 87–92.

Seyfried, W.E.J., Pester, N.J., Tutolo, B.M., Ding, K., 2015. The lost City hydrothermal system: constraints imposed by fluid chemistry and reaction path models on subseafloor heat and mass transfer processes. Geochim. Cosmochim. Acta 163, 59–79. https://doi.org/10.1016/j.gca.2015.04.040.

Sillén, L.G., 1967. Master variables and activity scales. In: Stumm, W. (Ed.), Equilibrium concepts in natural water systems, Volume 67 of advances in Chemistry Series. American Chemical Society, pp. 45–56.

Simon, L., Génin, J.M.R., Refait, P., 1997. Standard free enthalpy of formation of Fe(II)-Fe(III) hydroxysulphite green rust one and its oxidation into hydroxysulphate green rust two. Corros. Sci. 39, 1673–1685.

Sparks, D.L., 2003. Environmental Soil Chemistry. Academic Press, Elsevier Science.

Stampfl, P., 1969. Ein basisches Eisen-II-III-Karbonat in Rost. Corros. Sci. 9, 185–187.

Stein, E., Cohe, Y., Winer, A., 1996. Environmental distribution and transformation of mercury compounds – critical review. Environ. Sci. Technol. 26, 1–43.

Stone, D., Goldstein, R., 2004. Tubular precipitation and redox gradients on a bubbling template. Proc. Natl. Acad. Sci. 101, 11537–11541.

Sun, Z., Mu, S., Ye, X., Sun, Y., 1995. A microstructural tubular amakinite. Chin. Sci. Bull. 40, 1081–1084.

Sviridov, V., Yakovlevskaya, T., 1973. New data on amakinite from the kimberlitic pipe "Udachnaya" (in russian). Izvestiya Akademii Nauk SSSR. Ser. Geolog. 10, 144–147.

Taylor, R., 1981. Colour in soils and sediments - a review. In: Van Olphen, H., Veniale, F. (Eds.), International Clay Conference 1981. Elsevier, pp. 749–761.

Taylor, R., McKenzie, R., 1980. The influence of aluminum on iron oxides. VI. The formation of Fe(II)-Al(III) hydroxy-chlorides, −sulfates, and -carbonates as new members of the pyroaurite group and their significance in soils. Clay Clay Miner. 28, 179–187.

Templeton, A.S., Ellison, E.T., 2020. Formation and loss of metastable brucite: does Fe(II) bearing brucite support microbial activity in sepentinizing ecosystems. Philos. Transact. Royal Soc. London 378. https://doi.org/10.1098/rsta.2018.0423.

Trolard, F., 2006. Fougerite: from field experiment to the homologation of the mineral. Compt. Rendus Geosci. 338, 1158–1166.

Trolard, F., Bourrié, G., 1999. L'influence des oxydes de fer de type "rouilles vertes" sur les séquences d'oxydo-réduction dans les sols. Comptes Rendus de l'Académie des Sciences, Paris 329, 801–806.

Trolard, F., Bourrié, G., 2008. Geochemistry of green rusts and fougerite: A reevaluation of Fe cycle in soils. In: Sparks, D. (Ed.), Advances in Agronomy, 99. Elsevier, Amsterdam, pp. 228–288 chapter 5.

Trolard, F., Bourrié, G., 2012. Fougerite a natural layered double hydroxide in gley soil: habitus, structure, and some properties. In: Valášková, M., Martynková, G.S. (Eds.), Clay Minerals in Nature - their Characterization, Modification and Application. InTechOpen, pp. 171–188. URL. http://www.intechopen.com/books/.

Trolard, F., Abdelmoula, M., Bourrié, G., Humbert, B., Génin, J.M.R., 1996. Mise en évidence d'un constituant de type "rouilles vertes" dans les sols hydromorphes. Proposition de l'existence d'un nouveau minéral : la "fougérite". Comptes Rendus de l'Académie des Sciences, Paris 323, 1015–1022.

Trolard, F., Génin, J.M.R., Abdelmoula, M., Bourrié, G., Humbert, B., Herbillon, A., 1997. Identification of green rust mineral in a reductomorphic soil by Mössbauer and Raman spectroscopies. Geochim. Cosmochim. Acta 61, 1107–1111.

Trolard, F., Bourrié, G., Abdelmoula, M., Refait, P., Feder, F., 2007. Fougerite, a new mineral of the pyroaurite – iowaite group: description and crystal structure. Clay Clay Miner. 3, 323–334.

US Soil Survey Staff, 2010. Keys to Soil Taxonomy, 11 ed. USDA, NRCS.

Usman, M., Chaudhary, A., Orsetti, S., Hanna, K., Ruby, C., Kappler, A., Haderlein, S., 2018. Magnetite and green rust: synthesis, properties and environmental applications of mixed-valent iron minerals. Chem. Rev. 118, 3251–3304.

Vysotskii, G.N., 1999. Gley, an abridged publication of Vysotskii 1905 on the 257th anniversary of the Russian Academy of Sciences. In: Eurasian Soil Science, 32, pp. 1063–1068. Translated from Pochvovedenie, 10, 1999, 1189–1195, first published in russian in Pochvovedenie, 1905, 4, 291–327.

White, L.M., Shibuya, T., Vance, S.D., Christensen, L.E., Bhartia, R., Kidd, R., Hoffmann, A., Stucky, G.D., Kanik, I., Russell, M.J., 2020. Simulating serpentinization as it could apply to the emergence of life using the JPL hydrothermal reactor. Astrobiology 20, 307–326. URL. https://doi.org/10.1089/ast.2018.1949. pMID: 32125196 (web archive link,).

Williams, R.J.P., Fraústo da Silva, J.J.R., 1997. The Natural Selection of the Chemical Elements. Clarendon Press.

Williams, A., Scherer, M., 2001. Kinetics of Cr(VI) reduction by carbonate green rust. Environ. Sci. Technol. 35, 3488–3494.

Zegeye, A., Ona-Nguema, G., Carteret, C., Huguet, L., Abdelmoula, M., Jorand, F., 2005. Formation of hydroxysulphate green rust 2 as a single iron (II)–(III) mineral in microbial culture. Geomicrobiol J. 22, 389–399.

Zegeye, A., Bonneville, S., Benning, L.G., Sturm, A., Fowle, D.A., Jones, C., Canfield, D.E., Ruby, C., MacLean, L.C., Nomosatryo, S., Crowe, S.A., Poulton, S.W., 2012. Green rust formation controls nutrient availability in a ferruginous water column. Geology 40, 599–602.

Zhang, Z., Messan, O., Fang, J., Jackson, W.A., 2021. Abiotic reduction of nitrate and chlorate by Green rust. Am. Chem. Soc. Earth Space Chem. https://doi.org/10.1021/acsearthspacechem.1c00121.